1 Robust Minimum Variance Beamforming

R. G. Lorenz and S. P. Boyd

Beceem Communications, Santa Clara, CA
Stanford University, Stanford, CA

1.1 INTRODUCTION

Consider the n dimensional sensor array depicted in Fig. 1. Let $a(\theta) \in \mathbf{C}^n$ denote the response of the array to a plane wave of unit amplitude arriving from direction θ; we shall refer to $a(\cdot)$ as the *array manifold.* We assume that a narrow-band source $s(t)$ is impinging upon the array from angle θ and that the source is in the far-field of the array. The vector array output $y(t) \in \mathbf{C}^n$ is then:

$$y(t) = a(\theta)s(t) + v(t), \tag{1.1}$$

where $a(\theta)$ includes effects such as coupling between elements and subsequent amplification; $v(t)$ is a vector of additive noises representing the effect of undesired signals, such as thermal noise or interference. We denote the sampled array output by $y(k)$. Similarly, the combined beamformer output is given by

$$y_c(k) = w^* y(k) = w^* a(\theta)s(k) + w^* v(k)$$

where $w \in \mathbf{C}^n$ is a vector of weights, *i.e.*, design variables, and $(\cdot)^*$ denotes the conjugate transpose.

The goal is to make $w^* a(\theta) \approx 1$ and $w^* v(t)$ small, in which case, $y_c(t)$ recovers $s(t)$, *i.e.*, $y_c(t) \approx s(t)$. The gain of the weighted array response in direction θ is $|w^* a(\theta)|$; the expected effect of the noise and interferences at the combined output is given by $w^* R_v w$, where $R_v = \mathbf{E}\, vv^*$ and $\mathbf{E}$ denotes the expected value. If we presume $a(\theta)$

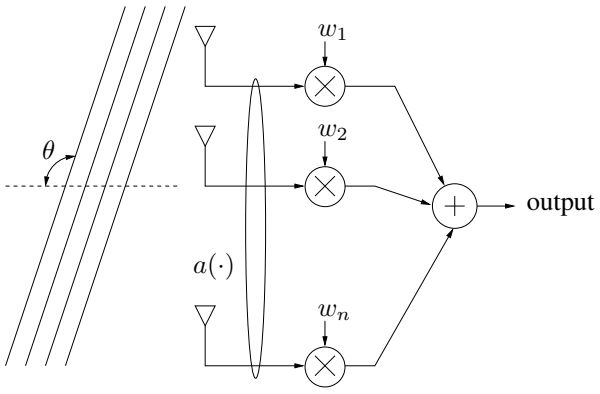

Fig. 1.1 Beamformer block diagram.

and R_v are known, we may choose w as the optimal solution of

$$\begin{array}{ll} \text{minimize} & w^* R_v w \\ \text{subject to} & w^* a(\theta_d) = 1. \end{array} \tag{1.2}$$

Minimum variance beamforming is a variation on (1.2) in which we replace R_v with an estimate of the received signal covariance derived from recently received samples of the array output, *e.g.*,

$$R_y = \frac{1}{N} \sum_{i=k-N+1}^{k} y(i) y(i)^* \in \mathbf{C}^{n \times n}. \tag{1.3}$$

The minimum variance beamformer (MVB) is chosen as the optimal solution of

$$\begin{array}{ll} \text{minimize} & w^* R_y w \\ \text{subject to} & w^* a(\theta) = 1. \end{array} \tag{1.4}$$

This is commonly referred to as Capon's method [10]. Equation (1.4) has an analytical solution given by

$$w_{\mathrm{mv}} = \frac{R_y^{-1} a(\theta)}{a(\theta)^* R_y^{-1} a(\theta)}. \tag{1.5}$$

Equation (1.4) also differs from (1.2) in that the power expression we are minimizing includes the effect of the desired signal plus noise. The constraint $w^* a(\theta) = 1$ in (1.4) prevents the gain in the direction of the signal from being reduced.

A measure of the effectiveness of a beamformer is given by the signal-to-interference-plus-noise ratio, commonly abbreviated as SINR, given by

$$\mathrm{SINR} = \frac{\sigma_{\mathrm{d}}^2 |w^* a(\theta)|^2}{w^* R_v w}, \tag{1.6}$$

where σ_{d}^2 is the power of the signal of interest. The assumed value of the array manifold $a(\theta)$ may differ from the actual value for a host of reasons including imprecise knowledge of the signal's angle of arrival θ. Unfortunately, the SINR of Capon's method can degrade catastrophically for modest differences between the assumed and actual values of the array manifold. We now review several techniques for minimizing the sensitivity of MVB to modeling errors in the array manifold.

1.1.1 Previous work

One popular method to address uncertainty in the array response or angle of arrival is to impose a set of unity-gain constraints for a small spread of angles around the nominal look direction. These are known in the literature as point mainbeam constraints or neighboring location constraints [25]. The beamforming problem with point mainbeam constraints can be expressed as

$$\begin{array}{ll} \text{minimize} & w^* R_y w \\ \text{subject to} & C^* w = f, \end{array} \tag{1.7}$$

where C is a $n \times L$ matrix of array responses in the L constrained directions and f is an $L \times 1$ vector specifying the desired response in each constrained direction. To achieve wider responses, additional constraint points are added. We may similarly constrain the derivative of the weighted array output to be zero at the desired look angle. This constraint can be expressed in the same framework as (1.7); in this case, we let C be the derivative of the array manifold with respect to look angle and $f = 0$. These are called *derivative mainbeam constraints;* this derivative may be approximated using regularization methods. Point and derivative mainbeam constraints may also be used in conjunction with one another. The minimizer of (1.7) has an analytical solution given by:

$$w_{\mathrm{opt}} = R_y^{-1} C (C^* R_y^{-1} C)^{-1} f. \tag{1.8}$$

Each constraint removes one of the remaining degrees of freedom available to reject undesired signals; this is particularly significant for an array with a small number of elements. We may overcome this limitation by using a low-rank approximation to the constraints [24]. The best rank k approximation to C, in a least squares sense, is given by $U \Sigma V^*$, where Σ is a diagonal matrix consisting of the largest k singular values, U is a $n \times k$ matrix whose columns are the corresponding left singular vectors of C, and V is a $L \times k$ matrix whose columns are the corresponding right singular vectors of C. The reduced rank constraint equations can be written as $V \Sigma^T U^* w = f$,

or equivalently:

$$U^*w = \Sigma^\dagger V^* f, \tag{1.9}$$

where † denotes the Moore-Penrose pseudoinverse. Using (1.8), we compute the beamformer using the reduced rank constraints as

$$w_{\rm epc} = R_y^{-1}U(U^*R_y^{-1}U)^{-1}\Sigma^\dagger V^* f.$$

This technique, used in source localization, is referred to as minimum variance beamforming with environmental perturbation constraints (MV-EPC), see [25] and the references contained therein.

Unfortunately, it is not clear how best to pick the additional constraints, or, in the case of the MV-EPC, the rank of the constraints. The effect of additional constraints on the design specifications appears difficult to predict.

Regularization methods [37] have also been used in beamforming. One technique, referred to in the literature as diagonal loading, chooses the beamformer to minimize the sum of the weighted array output power plus a penalty term, proportional to the square of the norm of the weight vector. The gain in the assumed angle of arrival (AOA) of the desired signal is constrained to be unity. The beamformer is chosen as the optimal solution of:

$$\begin{array}{ll} \text{minimize} & w^*R_y w + \mu w^* w \\ \text{subject to} & w^* a(\theta) = 1. \end{array} \tag{1.10}$$

The parameter $\mu > 0$ penalizes large values of w and has the general effect of *detuning* the beamformer response. The regularized least squares problem (1.10) has an analytical solution given by:

$$w_{\rm reg} = \frac{(R_y + \mu I)^{-1}a(\theta)}{a(\theta)^*(R_y + \mu I)^{-1}a(\theta)}. \tag{1.11}$$

Gershman [15] and Johnson and Dudgeon [22] provide a survey of these methods; see also the references contained therein. Similar ideas have been used in adaptive algorithms, see [20].

Beamformers using eigenvalue thresholding methods to achieve robustness have also been used; see [19]. The beamformer is computed according to Capon's method, using a covariance matrix which has been modified to ensure no eigenvalue is less than a factor μ times the largest, where $0 \leq \mu \leq 1$. Specifically, let $V\Lambda V^*$ denote the eigenvalue/eigenvector decomposition of R_y, where Λ is a diagonal matrix, the ith entry (eigenvalue) of which is given by λ_i, *i.e.*,

$$\Lambda = \begin{bmatrix} \lambda_1 & & \\ & \ddots & \\ & & \lambda_n \end{bmatrix}.$$

Without loss of generality, assume $\lambda_1 \geq \lambda_2 \ldots \geq \lambda_n$. We form the diagonal matrix Λ_{thr}, the ith entry of which is given by $\max\{\mu\lambda_1, \lambda_i\}$; *viz.*,

$$\Lambda_{\mathrm{thr}} = \begin{bmatrix} \lambda_1 & & & \\ & \max\{\mu\lambda_1, \lambda_2\} & & \\ & & \ddots & \\ & & & \max\{\mu\lambda_1, \lambda_n\} \end{bmatrix}.$$

The modified covariance matrix is computed according to $R_{\mathrm{thr}} = V\Lambda_{\mathrm{thr}}V^*$. The beamformer using eigenvalue thresholding is given by

$$w_{\mathrm{thr}} = \frac{R_{\mathrm{thr}}^{-1}a(\theta)}{a(\theta)^* R_{\mathrm{thr}}^{-1}a(\theta)}. \tag{1.12}$$

The parameter μ corresponds to the reciprocal of the condition number of the covariance matrix. A variation on this approach is to use a fixed value for the minimum eigenvalue threshold. One interpretation of this approach is to incorporate a-priori knowledge of the presence of additive white noise when the sample covariance is unable to observe said white noise floor due to short observation time [19]. The performance of this beamformer appears similar to that of the regularized beamformer using diagonal loading; both usually work well for an appropriate choice of the regularization parameter μ.

We see two limitations with regularization techniques for beamformers. First, it is not clear how to efficiently pick μ. Second, this technique does not take into account any knowledge we may have about variation in the array manifold, *e.g.*, that the variation may not be isotropic.

In §1.1.3, we describe a beamforming method that explicitly uses information about the variation in the array response $a(\cdot)$, which we model explicitly as an uncertainty ellipsoid in $\mathbf{R}^{2n}$. Prior to this, we introduce some notation for describing ellipsoids.

1.1.2 Ellipsoid descriptions

An n-dimensional ellipsoid can be defined as the image of an n-dimensional Euclidean ball under an affine mapping from $\mathbf{R}^n$ to $\mathbf{R}^n$; *i.e.*,

$$\mathcal{E} = \{Au + c \mid \|u\| \leq 1\}, \tag{1.13}$$

where $A \in \mathbf{R}^{n\times n}$ and $c \in \mathbf{R}^n$. The set $\mathcal{E}$ describes an ellipsoid whose center is c and whose *principal semiaxes* are the unit-norm left singular vectors of A scaled by the corresponding singular values. We say that an ellipsoid is *flat* if this mapping is not injective, *i.e.*, one-to-one. Flat ellipsoids can be described by (1.13) in the proper affine subspaces of $\mathbf{R}^n$. In this case, $A \in \mathbf{R}^{n\times l}$ and $u \in \mathbf{R}^l$. An interpretation of a flat uncertainty ellipsoid is that some linear combinations of the array manifold are known exactly [5].

Unless otherwise specified, an ellipsoid in $\mathbf{R}^n$ will be parameterized in terms of its center $c \in \mathbf{R}^n$ and a symmetric non-negative definite configuration matrix $Q \in \mathbf{R}^{n\times n}$ as

$$\mathcal{E}(c, Q) = \{Q^{1/2}u + c \mid \|u\| \leq 1\} \tag{1.14}$$

where $Q^{1/2}$ is any matrix square root satisfying $Q^{1/2}(Q^{1/2})^T = Q$. When Q is full rank, the non-degenerate ellipsoid $\mathcal{E}(c, Q)$ may also be expressed as

$$\mathcal{E}(c, Q) = \{x \mid (x - c)^T Q^{-1}(x - c) \leq 1\} \tag{1.15}$$

or by the equivalent quadratic function

$$\mathcal{E}(c, Q) = \{x \mid T(x) \leq 0\}, \tag{1.16}$$

where $T(x) = x^T Q^{-1}x - 2c^T Q^{-1}x + x_c^T Q^{-1}x_c - 1$. The first representation (1.14) is more natural when $\mathcal{E}$ is degenerate or poorly conditioned. Using the second description (1.15), one may easily determine whether a point lies within the ellipsoid. The third representation (1.16) will be used in §1.6.1 to compute the minimum-volume ellipsoid covering the union of ellipsoids.

We will express the values of the array manifold $a \in \mathbf{C}^n$ as the direct sum of its real and imaginary components in $\mathbf{R}^{2n}$; *i.e.*,

$$z_i = [\, \mathbf{Re}(a_1) \; \cdots \; \mathbf{Re}(a_n) \; \mathbf{Im}(a_1) \; \cdots \; \mathbf{Im}(a_n)]^T . \tag{1.17}$$

While it is possible to cover the field of values with a complex ellipsoid in $\mathbf{C}^n$, doing so implies a symmetry between the real and imaginary components which generally results in a larger ellipsoid than if the direct sum of the real and imaginary components are covered in $\mathbf{R}^{2n}$.

1.1.3 Robust minimum variance beamforming

A generalization of (1.4) that captures our desire to minimize the weighted power output of the array in the presence of uncertainties in $a(\theta)$ is then:

$$\begin{array}{ll} \text{minimize} & w^* R_y w \\ \text{subject to} & \mathbf{Re}\; w^* a \geq 1 \;\; \forall a \in \mathcal{E}, \end{array} \tag{1.18}$$

where $\mathbf{Re}$ denotes the real part. Here, $\mathcal{E}$ is an ellipsoid that covers the possible range of values of $a(\theta)$ due to imprecise knowledge of the array manifold $a(\cdot)$, uncertainty in the angle of arrival θ, or other factors. We shall refer to the optimal solution of (1.18) as the robust minimum variance beamformer (RMVB).

We use the constraint $\mathbf{Re}\; w^* a \geq 1$ for all $a \in \mathcal{E}$ in (1.18) for two reasons. First, while normally considered a semi-infinite constraint, we show in §1.3 that it can be expressed as a second-order cone constraint. As a result, the robust minimum variance beamforming problem (1.18) can be solved reliably and efficiently. Second, the real part of the response is an efficient lower bound for the magnitude of the

response, as the objective $w^* R_y w$ is unchanged if the weight vector w is multiplied by an arbitrary shift $e^{j\phi}$. This is particularly true when the uncertainty in the array response is relatively small. It is unnecessary to constrain the imaginary part of the response to be nominally zero.

Our approach differs from the previously mentioned beamforming techniques in that the weight selection uses the a-priori uncertainties in the array manifold in a precise way; the RMVB is guaranteed to satisfy the minimum gain constraint for all values in the uncertainty ellipsoid.

Recently, several papers have addressed uncertainty in a similar framework. Wu and Zhang [43] observe that the array manifold may be described as a polyhedron and that the robust beamforming problem can be cast as a quadratic program. While the polyhedron approach is less conservative, the size of the description and hence the complexity of solving the problem grows with the number of vertices. Vorobyov et al. [40], [41], and [16] describe the use of second-order cone programming for robust beamforming in the case where the uncertainty is in the array response is isotropic, *i.e.*, a Euclidean ball. Our method, while derived differently, yields the same beamformer as proposed by Li et al. [35], [29], [28].

In this chapter, we consider the case in which the uncertainty is anisotropic [33], [32], [31]. We also show how the beamformer weights can be computed efficiently.

1.1.4 Outline of the chapter

The rest of this chapter is organized as follows. In §1.2, we motivate the need for robustness with a simple array which includes the effect of coupling between antenna elements. In §1.3 we discuss the RMVB. A numerically efficient technique based on Lagrange multiplier methods is described; we will see that the RMVB can be computed with the same order of complexity as its non-robust counterpart. A numerical example is given in §1.4. In §1.5 we describe ellipsoidal modeling methods which make use of simulated or measured values of the array manifold. In §1.6 we discuss more sophisticated techniques, based on ellipsoidal calculus, for propagating uncertainty ellipsoids. In particular, we describe a numerically efficient method for approximating the numerical range of the Hadamard (element-wise) product of two ellipsoids. This form of uncertainty arises when the array outputs are subject to multiplicative uncertainties. A numerical beamforming example considering multiplicative uncertainties is given in §1.7. Our conclusions are given in §1.8.

1.2 A PRACTICAL EXAMPLE

Our goals for this section are twofold:

- to make the case that antenna elements may behave *very* differently in free space than as part of closely spaced arrays, and
- to motivate the need for robustness in beamforming.

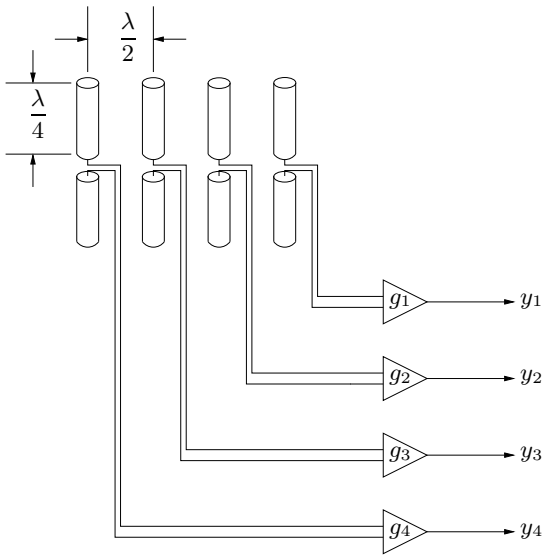

Fig. 1.2 The four-element array. For this array, we simulate the array response which includes the effect of coupling between elements. In this example, the gains $g_1, \ldots, g_4$ are all assumed nominal. Later we consider the effect of multiplicative uncertainties.

Consider the four-element linear array of half-wave dipole antennas depicted in Figure 1.2. Let the frequency of operation be 900 MHz and the diameter of the elements be 1.67 mm. Assume each dipole is terminated into a 100 ohm load. The length of the dipole elements was chosen such that an isolated dipole in free space matched this termination impedance.

The array was simulated using the Numerical Electromagnetics Code, version 4 (NEC-4) [9]. Each of the radiating elements was modeled with six wire segments. The nominal magnitude and phase responses are given in Figures 1.3 and 1.4, respectively. Note that the amplitude is *not* constant for all angles of arrival or the same for all elements. This will generally be the case with closely spaced antenna elements due to the high level of inter-element coupling.

In Figure 1.5, we see that the vector norm of the array response is *not* a constant function of AOA, despite the fact that the individual elements, in isolation, have an isotropic response.

Next, let us compare the performance of the RMVB with Capon's method using this array, with nominal termination impedances. Assume the desired signal impinges on the array from an angle $\theta_{\rm sig} = 127^\circ$ and has a signal-to-noise ratio (SNR) of 20 decibels (dB). We assume that an interfering signal arrives at an angle of $\theta_{\rm int} = 150^\circ$ with amplitude twice that of the desired signal. For Capon's method, we assume an AOA of $\theta_{\rm nom} = 120^\circ$. For the RMVB, we compute a minimum-volume ellipsoid

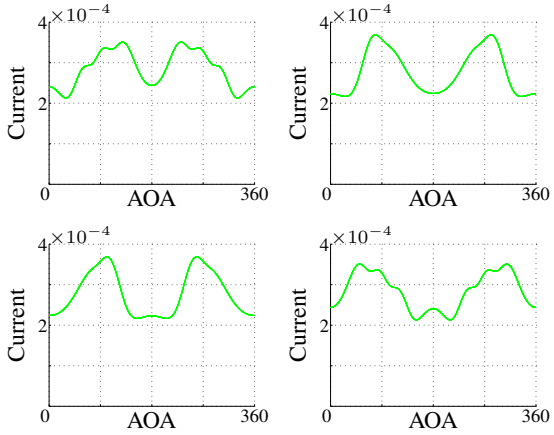

Fig. 1.3 Magnitude of response of four-element array consisting of half-wave dipoles with uniform spacing of $\frac{\lambda}{2}$. The currents have units of amperes for a field strength of 1 volt/meter. The angle of arrival (AOA) is in degrees. Note the symmetry of the response. The outer elements correspond to the top left and bottom right plots; the inner elements, top right and lower left.

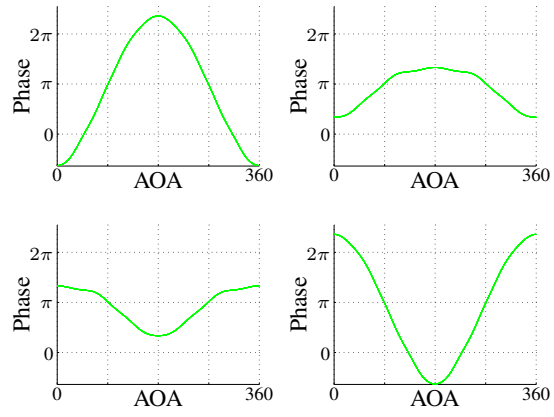

Fig. 1.4 Phase response, in radians, of the four-element half-wave dipole array. The angle of arrival is in degrees. Again, note the symmetry in the response.

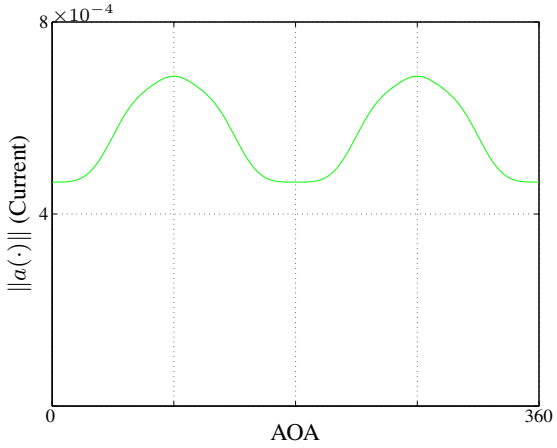

Fig. 1.5 The vector norm of the array response as a function of AOA. Note that the norm is not constant despite the fact that each of the elements are isotropic with respect to AOA.

covering the numerical range of the array manifold for all angles of arrival between 112° and 128°. The details of this calculation will be described in §1.5. Let $w_{\rm mv} \in \mathbf{C}^4$ denote the beamformer vector produced by Capon's method and $w_{\rm rmvb} \in \mathbf{C}^4$ the robust minimum-variance beamformer, *i.e.*, the optimal solution of (1.18).

A plot of the response of the minimum-variance beamformer (MVB) and the robust minimum-variance beamformer (RMVB) as a function of angle of arrival is shown in Figure 1.6. By design, the response of the MVB has unity gain in the direction of the assumed AOA, *i.e.*, $w_{\rm mv}^* a(\theta_{\rm nom}) = 1$, where $a : \mathbf{R} \rightarrow \mathbf{C}^4$ denotes the array manifold. The MVB produces a deep null in the direction of the interference: $w_{\rm mv}^* a(\theta_{\rm int}) = -0.0061 + 0i$. Unfortunately, the MVB also strongly attenuates the desired signal, with $w_{\rm mv}^* a(\theta_{\rm sig}) = -0.0677 + 0i$. The resulting post-beamforming signal-to-interference-plus-noise ratio (SINR) is -10.5 dB,appreciably worse than the SINR obtained using a single antenna *without* beamforming.

While the robust beamformer does not cast as deep a null in the direction of the interfering signal, *i.e.*, $w_{\rm rmvb}^* a(\theta_{\rm int}) = -0.0210 + 0i$, it maintains greater than unity gain for all angles of arrival in our design specification. The SINR obtained using the RMVB is 12.4 dB.

When the actual AOA of the desired signal equals the assumed 120°, the SINR of the MVB is an impressive 26.5 dB, compared to 10.64 dB for the RMVB. It is tempting then to consider methods to reduce the uncertainty and potentially realize this substantial improvement in SINR. Such efforts are unlikely to be fruitful. For example, a 1° error in the assumed AOA reduces the SINR of Capon's method by more than 20 dB to 4.0 dB. Also, the mathematical values of the array model differ from the actual array response for a number of reasons, of which error in the assumed AOA is but one. In the presence of array calibration errors, variations due to

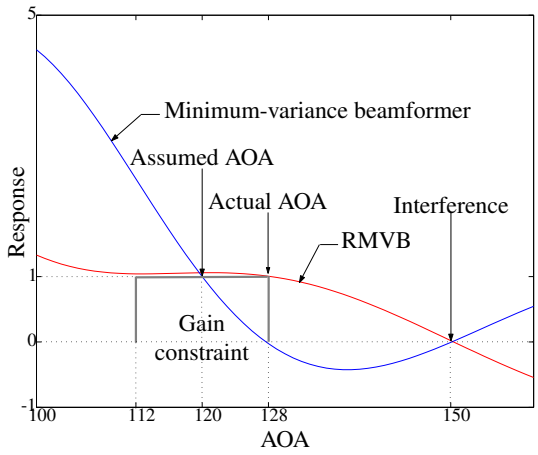

Fig. 1.6 The response of the minimum-variance beamformer (Capon's method) and the robust minimum-variance beamformer (RMVB). The a-priori uncertainty in the angle of arrival (AOA) was $\pm 8^\circ$. We see that the RMVB maintains at least unity gain for all angles in this range, whereas Capon's method fails for an AOA of approximately 127°.

termination impedances, and multiplicative gain uncertainties, non-robust techniques simply don't work reliably.

In our example, we considered only uncertainty in the angle of arrival; verifying the performance for the non-robust method involved evaluating points in a one-dimensional interval. Had we considered the additional effect of multiplicative gain variations, for example, the numerical cost of verifying the performance of the beamformer for a dense grid of possible array values could dwarf the computational complexity of the robust method. The approach of the RMVB is different; it makes specific use of the uncertainty in the array response. We compute either a worst-case optimal vector for the ellipsoidal uncertainty region or a proof that the design specification is infeasible. No subsequent verification of the performance is required.

1.3 ROBUST WEIGHT SELECTION

Recall from §1.1 that the RMVB was the optimal solution to

$$\begin{array}{ll} \text{minimize} & w^* R_y w \\ \text{subject to} & \mathbf{Re}\ w^* a \geq 1 \ \ \forall a \in \mathcal{E}. \end{array} \tag{1.19}$$

For purposes of computation, we will express the weight vector w and the values of the array manifold a as the direct sum of the corresponding real and imaginary

components

$$x = \begin{bmatrix} \mathbf{Re}\, w \\ \mathbf{Im}\, w \end{bmatrix} \qquad \text{and} \qquad z = \begin{bmatrix} \mathbf{Re}\, a \\ \mathbf{Im}\, a \end{bmatrix}. \tag{1.20}$$

The real and imaginary components of the product $w^* a$ can be expressed as

$$\mathbf{Re}\, w^* a = x^T z \tag{1.21}$$

and

$$\mathbf{Im}\, w^* a = x^T U z, \tag{1.22}$$

where U is the orthogonal matrix

$$U = \begin{bmatrix} 0 & I_n \\ -I_n & 0 \end{bmatrix},$$

and I_n is an $n \times n$ identity matrix. The quadratic form $w^* R_y w$ may be expressed in terms of x as $x^T R x$, where

$$R = \begin{bmatrix} \mathbf{Re}\, R_y & -\mathbf{Im}\, R_y \\ \mathbf{Im}\, R_y & \mathbf{Re}\, R_y \end{bmatrix}.$$

Assume R is positive definite; with sufficient sample support, it is with probability one.

Let $\mathcal{E} = \{Au + c \mid \|u\| \leq 1\}$ be an ellipsoid covering the possible values of x, *i.e.*, the real and imaginary components of a. The ellipsoid $\mathcal{E}$ is centered at c; the matrix A determines its size and shape. The constraint $\mathbf{Re}\ w^* a \geq 1$ for all $a \in \mathcal{E}$ in (1.18) can be expressed

$$x^T z \geq 1 \quad \forall z \in \mathcal{E}, \tag{1.23}$$

which is equivalent to

$$u^T A^T x \leq c^T x - 1 \ \text{ for all } \ u \ \text{ s.t. } \ \|u\| \leq 1. \tag{1.24}$$

Now, (1.24) holds for all $\|u\| \leq 1$ if and only if it holds for the value of u that maximizes $u^T A^T x$, namely $u = -\frac{A^T x}{\|A^T x\|}$. By the Cauchy-Schwartz inequality, we see that (1.23) is equivalent to the constraint

$$\|A^T x\| \ \leq c^T x - 1, \tag{1.25}$$

which is called a *second-order cone constraint* [30]. We can then express the robust minimum-variance beamforming problem (1.18) as

$$\begin{array}{ll} \text{minimize} & x^T R x \\ \text{subject to} & \|A^T x\| \leq c^T x - 1, \end{array} \tag{1.26}$$

which is a second-order cone program. See [30], [4], and [27]. The subject of robust convex optimization is covered in [8], [34], [13], [3], [2],and [5].

By assumption, R is positive definite and the constraint $\|A^T x\| \leq c^T x - 1$ in (1.26) precludes the trivial minimizer of $x^T R x$. Hence, this constraint will be tight for any optimal solution and we may express (1.26) in terms of real-valued quantities as

$$\begin{array}{ll} \text{minimize} & x^T R x \\ \text{subject to} & c^T x = 1 + \|A^T x\|. \end{array} \tag{1.27}$$

Compared to the MVB, the RMVB adds a margin that scales with the size of the uncertainty. In the case of no uncertainty where $\mathcal{E}$ is a singleton whose center is $c = [\mathbf{Re}\, a(\theta_d)^T \;\; \mathbf{Im}\, a(\theta_d)^T]^T$, (1.27) reduces to Capon's method and admits an analytical solution given by the MVB (1.5). Unlike the use of additional point or derivative mainbeam constraints or a regularization term, the RMVB is guaranteed to satisfy the minimum gain constraint for all values in the uncertainty ellipsoid. In the case of isotropic array uncertainty, the optimal solution of (1.18) yields the same weight vector (to a scale factor) as the regularized beamformer for the proper the proper choice of μ.

1.3.1 Lagrange multiplier methods

We may compute the RMVB efficiently using Lagrange multiplier methods. See, for example, [14], [18], [17, §12.1.1], and [6]. The RMVB is the optimal solution of

$$\begin{array}{ll} \text{minimize} & x^T R x \\ \text{subject to} & \|A^T x\|^2 = (c^T x - 1)^2 \end{array} \tag{1.28}$$

if we impose the additional constraint that $c^T x \geq 1$. We define the *Lagrangian* $L : \mathbf{R}^n \times \mathbf{R} \to \mathbf{R}$ associated with (1.28) as

$$\begin{aligned} L(x, \lambda) &= x^T R x + \lambda(\|A^T x\|^2 - (c^T x - 1)^2) \\ &= x^T (R + \lambda Q) x + 2\lambda c^T x - \lambda, \end{aligned} \tag{1.29}$$

where $Q = AA^T - cc^T$. To calculate the stationary points, we differentiate $L(x, y)$ with respect to x and λ; setting these partial derivatives equal to zero yields the Lagrange equations:

$$(R + \lambda Q)x = -\lambda c \tag{1.30}$$

and

$$x^T Q x + 2c^T x - 1 = 0. \tag{1.31}$$

To solve for the Lagrange multiplier λ, we note that equation (1.30) has an analytical solution given by

$$x = -\lambda (R + \lambda Q)^{-1} c;$$

applying this to (1.31) yields

$$\begin{aligned} f(\lambda) \;\; = \;\; & \lambda^2 c^T (R + \lambda Q)^{-1} Q (R + \lambda Q)^{-1} c \\ & -2\lambda c^T (R + \lambda Q)^{-1} c - 1. \end{aligned} \tag{1.32}$$

The optimal value of the Lagrange multiplier λ^* is then a zero of (1.32).
We proceed by computing the eigenvalue/eigenvector decomposition

$$V\Gamma V^T = R^{-1/2}Q(R^{-1/2})^T$$

to diagonalize (1.32), *i.e.*,

$$\begin{aligned} f(\lambda) &= \lambda^2\bar{c}^T(I+\lambda\Gamma)^{-1}\Gamma(I+\lambda\Gamma)^{-1}\bar{c} \\ &\quad -2\lambda\bar{c}^T(I+\lambda\Gamma)^{-1}\bar{c}-1, \end{aligned} \tag{1.33}$$

where $\bar{c} = V^T R^{-1/2}c$. Equation (1.33) reduces to the following scalar *secular* equation:

$$f(\lambda) = \lambda^2\sum_{i=1}^{n}\frac{\bar{c}_i^2\,\gamma_i}{(1+\lambda\,\gamma_i)^2} - 2\lambda\sum_{i=1}^{n}\frac{\bar{c}_i^2}{(1+\lambda\,\gamma_i)} - 1, \tag{1.34}$$

where $\gamma \in \mathbf{R}^n$ are the diagonal elements of Γ. The values of γ are known as the *generalized eigenvalues* of Q and R and are the roots of the equation $\det(Q-\lambda R) = 0$. Having computed the value of λ^* satisfying $f(\lambda^*) = 0$, the RMVB is computed according to

$$x^* = -\lambda^*(R+\lambda^* Q)^{-1}c. \tag{1.35}$$

Similar techniques have been used in the design of filters for radar applications; see Stutt and Spafford [36] and Abramovich and Sverdlik [1].
In principle, we could solve for all the roots of (1.34) and choose the one that results in the smallest objective value $x^T Rx$ *and* satisfies the constraint $c^T x > 1$, assumed in (1.28). In the next section, however, we show that this constraint is only met for values of the Lagrange multiplier λ greater than a minimum value, $\lambda_{\min}$. We will see that there is a single value of $\lambda > \lambda_{\min}$ that satisfies the Lagrange equations.

1.3.2 A lower bound on the Lagrange multiplier

We begin by establishing the conditions under which (9) has a solution. Assume $R = R^T \succ 0$, *i.e.*, R is symmetric and positive definite.

Lemma 1 *For $A \in \mathbf{R}^{n\times n}$ full rank, there exists an $x \in \mathbf{R}^n$ for which $\|A^T x\| = c^T x - 1$ if and only if $c^T(AA^T)^{-1}c > 1$.*

Proof: To prove the if direction, define

$$x(\lambda) = \left(cc^T - AA^T - \lambda^{-1}R\right)^{-1}c. \tag{1.36}$$

By the matrix inversion lemma, we have

$$\begin{aligned} c^T x(\lambda) - 1 &= c^T(cc^T - AA^T - \lambda^{-1}R)^{-1}c - 1 \\ &= \frac{1}{c^T(AA^T+\lambda^{-1}R)^{-1}c-1}. \end{aligned} \tag{1.37}$$

For $\lambda > 0$, $c^T(AA^T + \lambda^{-1}R)^{-1}c$ is a monotonically increasing function of λ; therefore, for $c^T(AA^T)^{-1}c > 1$, there exists a $\lambda_{\min} \in \mathbf{R}^+$ for which

$$c^T(AA^T + \lambda_{\min}^{-1}R)^{-1}c = 1. \tag{1.38}$$

This implies that the matrix $(R + \lambda_{\min}Q)$ is singular. Since

$$\begin{aligned} \lim_{\lambda\to\infty} c^T x(\lambda) - 1 &= -c^T(AA^T - cc^T)^{-1}c - 1 \\ &= \tfrac{1}{c^T(AA^T)^{-1}c-1} > 0, \end{aligned}$$

$c^T x(\lambda) - 1 > 0$ for all $\lambda > \lambda_{\min}$.
As in (1.32) and (1.34), let $f(\lambda) = \|A^T x\|^2 - (c^T x - 1)^2$. Examining (1.32), we see

$$\begin{aligned} \lim_{\lambda\to\infty} f(\lambda) &= -c^T(AA^T - cc^T)^{-1}c - 1 \\ &= \frac{1}{c^T(AA^T)^{-1}c - 1} > 0. \end{aligned}$$

Evaluating (1.32) or (1.34), we see $\lim_{\lambda\to\lambda_{\min}^+} f(\lambda) = -\infty$. For all $\lambda > \lambda_{\min}, c^T x > 1$ and $f(\lambda)$ is continuous. Hence $f(\lambda)$ assumes the value of 0, establishing the existence of a $\lambda > \lambda_{\min}$ for which $c^T x(\lambda) - 1 = \|A^T x(\lambda)\|$.
To show the only if direction, assume x satisfies $\|A^T x\| \le c^T x - 1$. This condition is equivalent to

$$z^T x \ge 1 \; \forall z \in \mathcal{E} = \{Au + c \mid \|u\| \le 1\}. \tag{1.39}$$

For (1.39) to hold, the origin cannot be contained in ellipsoid $\mathcal{E}$, which implies $c^T(AA^T)^{-1}c > 1$. □

Remark: The constraints $(c^T x - 1)^2 = \|A^T x\|^2$ and $c^T x - 1 > 0$ in (1.28), taken together, are equivalent to the constraint $c^T x - 1 = \|A^T x\|$ in (1.27). For $R = R^T \succ 0$, A full rank and $c^T(AA^T)^{-1}c > 1$, (1.27) has a unique minimizer x^*. For $\lambda > \lambda_{\min}$, $(\lambda^{-1}R + Q)$ is full rank, and the Lagrange equation (1.30)

$$(\lambda^{-1}R + Q)x^* = -c$$

holds for only a single value of λ. This implies there is a unique value of $\lambda > \lambda_{\min}$, for which the secular equation (1.34) equals zero.

Lemma 2 *For $x = -\lambda(R+\lambda Q)^{-1}c \in \mathbf{R}^n$ with $A \in \mathbf{R}^{n\times n}$ full rank, $c^T(AA^T)^{-1}c > 1$, and $\lambda > 0, c^T x > 1$ if and only if the matrix $(R + \lambda(AA^T - cc^T))$ has a negative eigenvalue.*

Proof: Consider the matrix

$$M = \begin{bmatrix} \lambda^{-1}R + AA^T & c \\ c^T & 1 \end{bmatrix}.$$

We define the inertia of M as the triple $In\{M\} = \{n_+, n_-, n_0\}$, where $n+$ is the number of positive eigenvalues, n_- is the number of negative eigenvalues, and n_0 is the number of zero eigenvalues of M. See Kailath et al. [23, pp.729-730].

Since both block diagonal elements of M are invertible,

$$\begin{aligned} In\{M\} &= In\{\lambda^{-1}R + AA^T\} + In\{\Delta_1\} \\ &= In\{1\} + In\{\Delta_2\}, \end{aligned} \tag{1.40}$$

where $\Delta_1 = 1 - c^T(\lambda^{-1}R + AA^T)^{-1}c$, the Schur complement of the (1,1) block in M, and $\Delta_2 = \lambda^{-1}R + AA^T - cc^T$, the Schur complement of the (2,2) block in M. We conclude $c^T(\lambda^{-1}R + AA^T)^{-1}c > 1$ if and only if the matrix $(\lambda^{-1}R + AA^T - cc^T)$ has a negative eigenvalue. By the matrix inversion lemma,

$$\frac{1}{c^T(\lambda^{-1}R + AA^T)^{-1}c - 1} = -c^T(\lambda^{-1}R + AA^T - cc^T)^{-1}c - 1. \tag{1.41}$$

Inverting a scalar preserves its sign, therefore,

$$c^T x - 1 = -c^T(\lambda^{-1}R + AA^T - cc^T)^{-1}c - 1 > 0 \tag{1.42}$$

if and only if $\lambda^{-1}R + AA^T - cc^T$ has a negative eigenvalue. □

Remark: Applying Sylvester's law of inertia to equations (1.32) and (1.34), we see that

$$\lambda_{\min} = -\frac{1}{\gamma_j}, \tag{1.43}$$

where γ_j is the single negative generalized eigenvalue. Using this fact and (1.34), we can readily verify $\lim_{\lambda \to \lambda_{\min}^+} f(\lambda) = -\infty$, as stated in Lemma 1.

Two immediate consequences follow from Lemma 2. First, we may exclude from consideration any value of λ less than $\lambda_{\min}$. Second, for all $\lambda > \lambda_{\min}$, the matrix $R + \lambda Q$ has a single negative eigenvalue. We now use these facts to obtain a tighter lower bound on the value of the optimal Lagrange multiplier.

We begin by rewriting (1.34) as

$$\sum_{i=1}^{n} \frac{\bar{c}_i^2(-2 - \lambda\gamma_i)}{(1 + \lambda\gamma_i)^2} = \frac{1}{\lambda}. \tag{1.44}$$

Recall exactly one of the generalized eigenvalues γ in the secular equation (1.44) is negative. We rewrite (1.44) as

$$\lambda^{-1} = \frac{\bar{c}_j^2(-2 - \lambda\gamma_j)}{(1 + \lambda\,\gamma_j)^2} - \sum_{i \neq j} \frac{\bar{c}_i^2(2 + \lambda\gamma_i)}{(1 + \lambda\gamma_i)^2} \tag{1.45}$$

where j denotes the index associated with this negative eigenvalue.

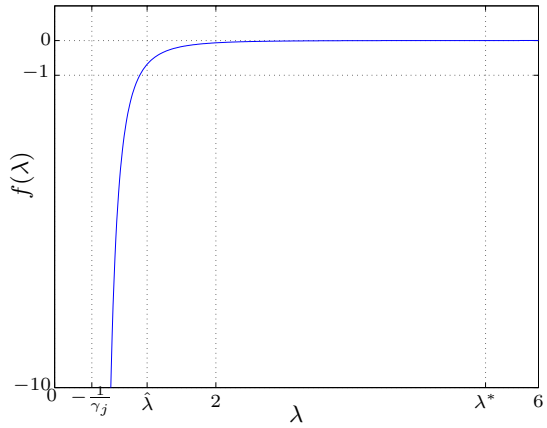

Fig. 1.7 Plot of the secular equation from the §1.2 example. Here γ_j is the (single) negative eigenvalue of $R^{-1/2}(AA^T - cc^T)(R^{-1/2})^T$, $\hat{\lambda}$ is the computed lower bound on the Lagrange multiplier, and λ^* the solution to the secular equation.

A lower bound on λ can be found by ignoring the terms involving the non-negative eigenvalues in (1.45) and solving

$$\lambda^{-1} = \frac{\bar{c}_i^2(-2 - \lambda\gamma_j)}{(1 + \lambda\gamma_j)^2}.$$

This yields a quadratic equation in λ

$$\lambda^2(\bar{c}_j^2\gamma_j + \gamma_j^2) + 2\lambda(\gamma_j + \bar{c}_j^2) + 1 = 0, \tag{1.46}$$

the roots of which are given by

$$\lambda = \frac{-1 \pm |\bar{c}_j|(\gamma_j + \bar{c}_j^2)^{-1/2}}{\gamma_j}. \tag{1.47}$$

By Lemma 2, the constraint $c^T x^* \geq 1$ implies $R + \lambda^* Q$ has a negative eigenvalue, since

$$\begin{aligned} c^T x^* &= c^T(-\lambda^*(R + \lambda Q)^{-1})c \quad \geq 1 \\ &= -\lambda^* \bar{c}^T(I + \lambda^*\Gamma)^{-1}\bar{c} \end{aligned}$$

Hence, $\lambda^* > -1/\gamma_j$ where γ_j is the single negative eigenvalue. We conclude $\lambda^* > \hat{\lambda}$, where

$$\hat{\lambda} = \frac{-1 - |\bar{c}_j|(\gamma_j + \bar{c}_j^2)^{-1/2}}{\gamma_j}. \tag{1.48}$$

In Figure 1.7 we see a plot of the secular equation and the improved lower bound $\hat{\lambda}$ found in (1.48).

1.3.3 Some technical details

In this section, we show that the parenthetical quantity in (1.48) is always non-negative for any feasible beamforming problem. We also prove that the lower bound on the Lagrange multiplier in (1.48 is indeed that.

Recall that for any feasible beamforming problem, $Q = AA^T - cc^T$ has a negative eigenvalue. Note that $\bar{c}_j = v_j^T R^{-\frac{1}{2}} c$, where v_j is the eigenvector associated with the negative eigenvalue γ_j. Hence, $v_j \in \mathbf{R}^n$ can be expressed as the optimal solution of

$$\begin{array}{ll} \text{minimize} & v^T R^{-\frac{1}{2}} (AA^T - cc^T) \left(R^{-\frac{1}{2}}\right)^T v \\ \text{subject to} & \|v\| = 1 \end{array} \tag{1.49}$$

and $\gamma_j = v_j^T R^{-\frac{1}{2}} (AA^T - cc^T) \left(R^{-\frac{1}{2}}\right)^T v_j$, the corresponding objective value. Since

$$\bar{c}_j^2 = v_j^T R^{-\frac{1}{2}} c \left(v_j^T R^{-\frac{1}{2}} c\right)^T = v_j^T R^{-\frac{1}{2}} cc^T \left(R^{-\frac{1}{2}}\right)^T v_j, \tag{1.50}$$

we conclude $(\gamma_j + \bar{c}_j^2) = v_j^T R^{-\frac{1}{2}} AA^T (R^{-\frac{1}{2}})^T v_j > 0$.

To show that there exists no root between $\lambda_{\min}$ and $\hat{\lambda}$, we rewrite the secular equation (1.34)

$$f(\lambda) = g(\lambda) + h(\lambda), \tag{1.51}$$

where

$$\begin{aligned} g(\lambda) &= \lambda^2 \frac{\bar{c}_j^2 \gamma_j}{(1+\lambda\gamma_j)^2} - 2\lambda \frac{\bar{c}_j^2}{(1+\lambda\gamma_j)} - 1 \\ &= \frac{\lambda^2(\bar{c}_j^2\gamma_j + \gamma_j^2) + 2\lambda(\gamma_j + \bar{c}_j^2) + 1}{-(1+\lambda\gamma_j)^2} \end{aligned} \tag{1.52}$$

and

$$\begin{aligned} h(\lambda) &= \lambda^2 \sum_{i \neq j} \frac{\bar{c}_j^2 \gamma_j}{(1+\lambda\gamma_j)^2} - 2\lambda \sum_{i \neq j} \frac{\bar{c}_j^2}{(1+\lambda\gamma_j)} \\ &= -\lambda \sum_{i \neq j} \frac{(\lambda\gamma_i + 2)(\gamma_i + \bar{c}_i^2)}{(1+\lambda\gamma_i)^2} \end{aligned} \tag{1.53}$$

Comparing (1.46) and (1.52), we see the roots of $g(\lambda)$ are given by (1.47). Since $g'(\lambda) < 0$ for all $\lambda < \frac{-1}{\gamma_j}$ and $\lim_{\lambda \to 0} g(\lambda) = -1$, there exists no solution to the secular equation for $\gamma \in [0, -\frac{1}{\gamma_j})$. Hence the unique root of $g(\lambda)$ is given by (1.48). Since all of the eigenvalues $\gamma_i,\ i \neq j$ in (1.52) are non-negative, $h(\lambda)$ is continuous, bounded and differentiable for all $\lambda > 0$. The derivative of the h with respect to λ is

given by

$$h'(\lambda) = -2\sum_{i\neq j}\frac{\bar{c}_i^2}{(1+\lambda\gamma_i)^3} \tag{1.54}$$

By inspection, $h'(\lambda) < 0$ for all $\lambda > 0$.

We now show that $\hat{\lambda}$ is a strict lower bound for the root of the secular equation (1.34). Define $t : \mathbf{R}\times\mathbf{R}\rightarrow\mathbf{R}$, according to:

$$t(\lambda,\theta) = g(\lambda) + \theta h(\lambda), \tag{1.55}$$

where $\theta \in [0,1]$. For $\theta = 0, t(\lambda,\theta) = g(\lambda)$; hence $t(\hat{\lambda},0)$, where $\hat{\lambda}$ is as in (1.48). As $g(\lambda)$ and $h(\lambda)$ are locally smooth and bounded, the total differential of t is given by

$$dt = \left(\frac{\partial g}{\partial\lambda} + \theta\frac{\partial h}{\partial\lambda}\right)d\lambda + h(\lambda)d\theta$$

The first order condition for the root t is given by:

$$\left(\frac{\partial g}{\partial\lambda} + \theta\frac{\partial h}{\partial\lambda}\right)d\lambda = -h(\lambda)d\theta.$$

Since $f(\lambda)$ is an increasing function of λ for all $\lambda \in [-1/\gamma_j, \lambda^*]$ and $h'(\lambda) < 0$ for all $\lambda > 0$, $\left(\frac{\partial g}{\partial\lambda} + \theta\frac{\partial h}{\partial\lambda}\right) > 0$ for all $\theta \in [0,1]$ and $\lambda \in [-1/\gamma_j, \lambda^*]$. Recall $h(\lambda) < 0$ for all $\lambda > 0$. Hence, as θ is increased, the value of λ satisfying $t(\theta,\lambda)$ increases. The value of λ satisfying $t(1,\lambda)$ is the solution to the secular equation, establishing that the (1.48) is a lower bound.

1.3.4 Solution of the secular equation

The secular equation (1.34) can be efficiently solved using the Newton-Raphson method. This method enjoys quadratic convergence if started sufficiently close to the root λ^*; see Dahlquist and Björck [11, §6] for details. The derivative of this secular equation with respect to λ is given by

$$f'(\lambda) = -2\sum_{i=1}^{n}\frac{\bar{c}_i^2}{(1+\lambda\gamma_i)^3}. \tag{1.56}$$

The secular equation (1.34) is not necessarily a monotonically increasing function of λ. A plot showing the convergence of the secular equation, from the §1.2 example, is shown in Figure 1.8.

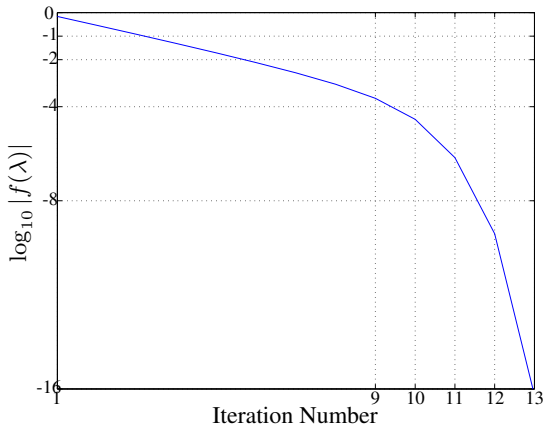

Fig. 1.8 Iterations of the secular equation. For λ sufficiently close to λ^*, in this case, after 9 iterations, the iterates converge quadratically, doubling the number of bits of precision at every iteration.

1.3.5 Summary and computational complexity of the RMVB computation

We summarize the algorithm below. In parentheses are approximate costs of each of the numbered steps; the actual costs will depend on the implementation and problem size [12]. As in [17] we will consider a flop to be any single floating-point operation.

RMVB computation

given R, strictly feasible A and c.

1. *Calculate* $Q \leftarrow AA^T - cc^T$. $(2n^2)$
2. *Change coordinates*. $(2n^3)$
   a. compute Cholesky factorization $LL^T = R$.
   b. compute $L^{-1/2}$.
   c. $\tilde{Q} \leftarrow L^{-1/2}Q(L^{-1/2})^T$.
3. *Eigenvalue/eigenvector computation*. $(10n^3)$
   a. compute $V\Gamma V^T = \tilde{Q}$.
4. *Change coordinates*. $(4n^2)$
   a. $\bar{c} \leftarrow V^T R^{-1/2} c$.
5. *Secular equation solution*. $(80n)$
   a. compute initial feasible point $\hat{\lambda}$
   b. find $\lambda^* > \hat{\lambda}$ for which $f(\lambda) = 0$.
6. *Compute* $x^* \leftarrow (R + \lambda^* Q)^{-1} c$ (n^3)

The computational complexity of these steps is discussed below:

1. Forming the matrix product AA^T is expensive and should be avoided. If the parameters of the uncertainty ellipsoid are stored, the shape parameter may be stored as AA^T. In the event that an aggregate ellipsoid is computed using the methods of §1.6, the quantity AA^T is produced. In either case, only the subtraction of the quantity cc^T need be performed, requiring $2n^2$ flops.

2. Computing the Cholesky factor L in step 2 requires $n^3/3$ flops. The resulting matrix is triangular, hence computing its inverse requires $n^3/2$ flops. Forming the matrix $\tilde{Q}$ in step 2.c requires n^3 flops.

3. Computing the eigenvalue/eigenvector decomposition is the most expensive part of the algorithm. In practice, it takes approximately $10n^3$ flops.

5. Solution of the secular equation requires minimal effort. The solution of the secular equation converges quadratically. In practice, the starting point $\hat{\lambda}$ is close to λ^*; hence, the secular equation generally converges in 7 to 10 iterations, independent of problem size.

6. Accounting for the symmetry in R and Q, computing x^* requires n^3 flops.

In comparison, the regularized beamformer requires n^3 flops. Hence the RMVB requires approximately 12 times the computational cost of the regularized beamformer. Note that this factor is independent of problem size.

In §1.6, we extend the methods of this section to the case of multiplicative uncertainties by computing an outer approximation to the element-wise or Hadamard product of ellipsoids. Using this approximation, no subsequent verification of the performance is required.

1.4 A NUMERICAL EXAMPLE

Consider a 10-element uniform linear array, centered at the origin, in which the spacing between the elements is half of a wavelength. Assume the response of each element is isotropic and has unit norm. If the coupling between elements is ignored, the response of the array $a : \mathbf{R} \rightarrow \mathbf{C}^{10}$ is given by:

$$a(\theta) = \left[\begin{array}{cccccc} e^{-9\phi/2} & e^{-7\phi/2} & \cdots & e^{7\phi/2} & e^{9\phi/2} \end{array} \right]^T,$$

where $\phi = \pi \cos(\theta)$ and θ is the angle of arrival. As seen in §1.2, the responses of closely spaced antenna elements may differ substantially from this model.

In this example, three signals impinge upon the array: a desired signal $s_{\rm d}(t)$ and two uncorrelated interfering signals $s_{\rm int1}(t)$ and $s_{\rm int2}$. The signal-to-noise ratio (SNR) of the desired signal at each element is 20 dB. The angles of arrival of the interfering signals, $\theta_{\rm int1}$ and $\theta_{\rm int2}$, are 30° and 75°; the SNRs of these interfering signals, 40dB and 20dB, respectively. We model the received signals as:

$$y(t) = a_{\rm d} s_{\rm d}(t) + a(\theta_{\rm int1}) s_{\rm int1}(t) + a(\theta_{\rm int2}) s_{\rm int2}(t) + v(t), \tag{1.57}$$

where $a_{\rm d}$ denotes the array response of the desired signal, $a(\theta_{\rm int1})$ and $a(\theta_{\rm int2})$, the array responses for the interfering signals, $s_{\rm d}(t)$ denotes the complex amplitude of the desired signal, $s_{\rm int1}(t)$ and $s_{\rm int2}(t)$, the interfering signals, and $v(t)$ is a complex vector of additive white noises.

Let the noise covariance $\mathbf{E}\, vv^* = \sigma_n^2 I$, where I is an $n \times n$ identity matrix and n is the number of antennas, *viz.*, 10. Similarly define the powers of the desired signal and interfering signals to be $\mathbf{E}\, s_{\rm d} s_{\rm d}^* = \sigma_{\rm d}^2$, $\mathbf{E}\, s_{\rm int1} s_{\rm int1}^* = \sigma_{\rm int1}^2$, and $\mathbf{E}\, s_{\rm int1} s_{\rm int2}^* = \sigma_{\rm int2}^2$, where

$$\frac{\sigma_{\rm d}^2}{\sigma_n^2} = 10^2, \qquad \frac{\sigma_{\rm int1}^2}{\sigma_n^2} = 10^4, \qquad \frac{\sigma_{\rm int2}^2}{\sigma_n^2} = 10^2.$$

If we assume the signals $s_{\rm d}(t), s_{\rm int1}(t), s_{\rm int2}(t)$, and $v(t)$ are all uncorrelated, the estimated covariance, which uses the actual array response, is given by

$$\mathbf{E}\, R = \mathbf{E}\, yy^* = \sigma_{\rm d}^2 a_{\rm d} a_{\rm d}^* + \sigma_{\rm int1}^2 a(\theta_{\rm int1}) a(\theta_{\rm int1})^* + \sigma_{\rm int2}^2 a(\theta_{\rm int2}) a(\theta_{\rm int2})^* + \sigma_{\rm n}^2 I. \tag{1.58}$$

In practice, the covariance of the received signals plus interference is often neither known nor stationary and hence must be estimated from recently received signals. As a result, the performance of beamformers is often degraded by errors in the covariance due to either small sample size or movement in the signal sources.

We will compare the performance of the robust beamformer with beamformers using two regularization techniques: diagonal loading and eigenvalue thresholding. In this example, we assume a-priori, that the nominal AOA, $\theta_{\rm nom}$, is 45°. The actual array response is contained in an ellipsoid $\mathcal{E}(c, P)$, whose center and configuration matrix are computed from N equally-spaced samples of the array response at angles between 40° and 50° according to

$$c = \frac{1}{N} \sum_{i=1}^{N} a(\theta_i) \qquad P = \frac{1}{\alpha N} \sum_{i=1}^{N} \left(a(\theta_i) - c\right) \left(a(\theta_i) - c\right)^*, \tag{1.59}$$

where

$$\theta_i = \theta_{\rm nom} + \left(-\frac{1}{2} + \frac{i-1}{N-1}\right) \Delta_\theta, \quad \text{for } i \in [1, N], \tag{1.60}$$

and

$$\alpha = \sup_{i \in [1,N]} (a(\theta_i) - c)^* P^{-1} (a(\theta_i) - c).$$

Here, $\Delta_\theta = 10^\circ$, and $N = 64$.

In Figure 1.9, we see the reception pattern of the array employing the MVB, the regularized beamformer (1.10), and the RMVB, all computed using the nominal AOA and the corresponding covariance matrix R. The regularization term used in the regularized beamformer was chosen to be $\frac{1}{100}$ of the largest eigenvalue of the received covariance matrix. By design, both the MVB and the regularized beamformer have unity gain at the nominal AOA. The response of the regularized beamformer is seen

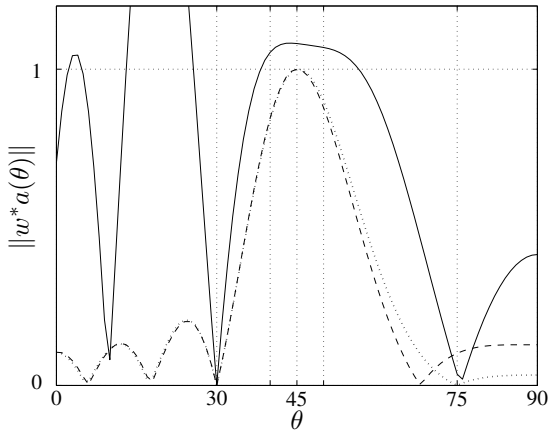

Fig. 1.9 The response of the MVB (Capon's method, dashed trace), the regularized beamformer employing diagonal loading (dotted trace), and the RMVB (solid trace) as a function of angle of arrival θ. Note that the RMVB preserves greater than unity gain for all angles of arrival in the design specification of $\theta \in [40, 50]$

to be a detuned version of the MVB. The RMVB maintains greater-than-unity gain for all AOAs covered by the uncertainty ellipsoid $\mathcal{E}(c, P)$.

In Figure 1.10 we see the effect of changes in the regularization parameter μ on the worst-case SINRs for the regularized beamformers using diagonal loading and eigenvalue thresholding, and the effect of scaling the uncertainty ellipsoid on the RMVB. Using the definition of SINR (1.6), we define the worst case SINR is as the minimum objective value of the following optimization problem:

$$\begin{array}{ll} \text{minimize} & \dfrac{\sigma_{\mathrm{d}}^2 \|w^* a\|^2}{\mathbf{E}\, w^* R_v w} \\ \text{subject to} & a \in \mathcal{E}(c, P), \end{array}$$

where the expected covariance of the interfering signals and noises is given by

$$\mathbf{E}\, R_v = \sigma_{\mathrm{int}1}^2 a(\theta_{\mathrm{int}1}) a(\theta_{\mathrm{int}1})^* + \sigma_{\mathrm{int}1}^2 a(\theta_{\mathrm{int}2}) a(\theta_{\mathrm{int}2})^* + \sigma_{\mathrm{n}}^2 I.$$

The weight vector w and covariance matrix of the noise and interfering signals R_v used in its computation reflect the chosen value of the array manifold.

For diagonal loading, the parameter μ is the scale factor multiplying the identity matrix added to the covariance matrix, divided by the largest eigenvalue of the covariance matrix R. For small values of μ, *i.e.*, 10^{-6}, the performance of the regularized beamformer approaches that of Capon's method; the worst-case SINR for Capon's method is -29.11 dB. As $\mu \to \infty, w_{reg} \to a(\theta_{\mathrm{nom}})$.

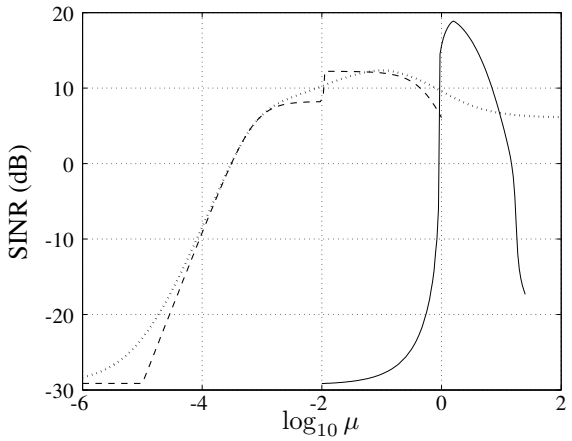

Fig. 1.10 The worst-case performance of the regularized beamformers based on diagonal loading (dotted) and eigenvalue thresholding (dashed) as a function of the regularization parameter μ. The effect of scaling of the uncertainty ellipsoid used in the design of the RMVB (solid) is seen; for $\mu = 1$ the uncertainty used in designing the robust beamformer equals the actual uncertainty in the array manifold.

The beamformer based on eigenvalue thresholding performs similarly to the beamformer based on diagonal loading. In this case, μ is defined to be the ratio of the threshold to the largest eigenvalue of R; as such, the response of this beamformer is only computed for $\mu \leq 1$.

For the robust beamformer, we use μ to define the ratio of the size of the ellipsoid used in the beamformer computation $\mathcal{E}_{\rm design}$ divided by size of the actual array uncertainty $\mathcal{E}_{\rm actual}$. Specifically, if $\mathcal{E}_{\rm actual} = \{Au+c \,|\, \|u\| \leq 1\}$, $\mathcal{E}_{\rm design} = \{\mu Av+c \,|\, \|v\| \leq 1\}$. When the design uncertainty equals the actual, the worst-case SINR of the robust beamformer is seen to be 15.63 dB. If the uncertainty ellipsoid used in the RMVB design significantly overestimates or underestimates the actual uncertainty, the worst-case SINR is decreased.

For comparison, the worst-case SINR of the MVB with (three) unity mainbeam constraints at $40°, 45°$, and $50°$ is 1.85 dB. The MV-EPC beamformer was computed using the same 64 samples of the array manifold as the computation of the uncertainty ellipsoid (1.59); the design value for the response in each of these directions was unity. The worst-case SINRs of the rank-1 through rank-4 MV-EPC beamformers were found to be -28.96 dB, -3.92 dB, 1.89 dB, and 1.56 dB, respectively. The worst-case response for the rank-5 and rank-6 MV-EPC beamformers is *zero*; *i.e.*, it can fail completely.

1.4.1 Power estimation

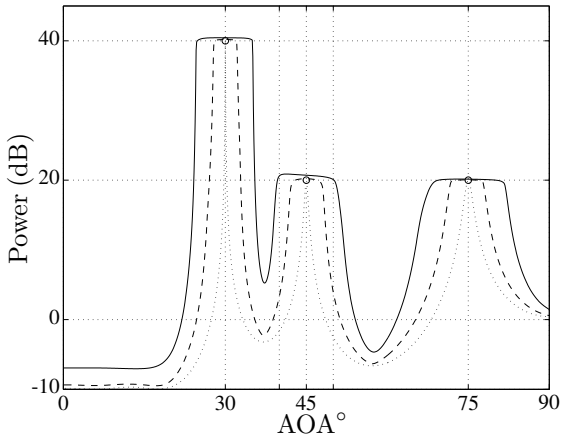

Fig. 1.11 The ambiguity function for RMVB beamformer using an uncertainty ellipsoid computed from a beamwidth of 10° (solid), 2° (dashed) and the Capon beamformer (dotted). The true powers of the signal of interest and interfering signals are denoted with circles. In this example, the additive noise power at each element has unit variance; hence, the ambiguity function corresponds to SNR.

If the signals and noises are all uncorrelated, the sample covariance, as computed in (1.3), equals its expected value, and the uncertainty ellipsoid contains the actual array response, the RMVB is guaranteed to have greater than unity magnitude response for all values of the array manifold in the uncertainty ellipsoid $\mathcal{E}$. In this case, an upper bound on the power of the desired signal, $\sigma_{\rm d}^2$, is simply the weighted power out of the array, namely

$$\hat{\sigma}_{\rm d}^2 = w^* R_y w. \tag{1.61}$$

In Figure 1.11, we see the square of the norm of the weighted array output as a function of the hypothesized angle of arrival $\theta_{\rm nom}$. for the RMVB using uncertainty ellipsoids computed according to (1.59) and (1.60) with $\Delta\theta = 10^\circ, 4^\circ$, and 0°. If the units of the array output correspond to volts or amperes, the square of the magnitude of the weighted array output has units of power. This plot is referred to in the literature as a spatial ambiguity function [29],[28]; its resolution is seen to decrease with increasing uncertainty ellipsoid size. The RMVB computed for $\Delta\theta = 0^\circ$ corresponds to the Capon beamformer. The spatial ambiguity function using the Capon beamformer provides an accurate power estimate only when the assumed array manifold equals the actual.

We summarize the effect of differences between assumed and actual uncertainty regions on the performance of the RMVB:

- If the assumed uncertainty ellipsoid equals the actual uncertainty, the gain constraint is met and no other choice of gain vector yields better worst-case performance over all values of the array manifold in the uncertainty ellipsoid.
- If the assumed uncertainty ellipsoid is smaller than the actual uncertainty, the minimum gain constraint will generally not be met for all possible values if the array manifold. If the uncertainty ellipsoid used in computing the RMVB is much smaller than the actual uncertainty, the performance may degrade substantially. The power estimate, computed using the RMVB as in (1.61) is not guaranteed to be an upper bound, even when an accurate covariance is used in the computation.
- If assumed uncertainty is greater than the actual uncertainty, the performance is generally degraded, but the minimum gain in desired look direction is maintained. Given accurate covariance, the appropriately scaled weighted power out of the array yields an upper bound on the power of the received signal.

The performance of the RMVB is not optimal with respect to SINR; it is optimal in the following sense. For a fixed covariance matrix R and an array response contained in an ellipsoid $\mathcal{E}$, no other vector achieves a lower weighted power out of the array while maintaining the real part of the response greater than unity for all values of the array contained in $\mathcal{E}$.

In the next section, we describe two methods for computing ellipsoids covering a collection of points.

1.5 ELLIPSOIDAL MODELING

The uncertainty in the response of an antenna array to a plane wave arises principally from three sources:

- uncertainty in the angle of arrival (AOA),
- uncertainty in the array manifold given perfect knowledge of the AOA (also called calibration errors), and
- variations in the gains of the signal-processing paths.

In this section, we describe methods to compute an ellipsoid that approximates or covers the range of possible values of the array manifold, given these uncertainties.

1.5.1 Ellipsoid computation using mean and covariance of data

If the array manifold is measured in a controlled manner, the ellipsoid describing it may be generated from the mean and covariance of the measurements from repeated trials. In the case where the array manifold is not measured but rather predicted from

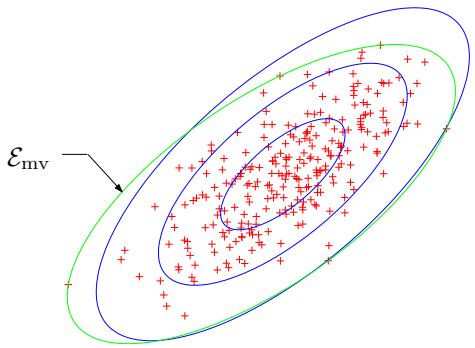

Fig. 1.12 A minimum-volume ellipsoid $\mathcal{E}_{\mathrm{mv}}$ covering points drawn from a bivariate normal distribution. The one-, two-, and 3-σ ellipsoids calculated from the first and second moments of the data are also shown.

numerical simulations, the uncertainty may take into account variation in the array response due to manufacturing tolerance, termination impedance, and similar effects. If the underlying distribution is multivariate normal, the k standard deviation $(k\sigma)$ ellipsoid would be expected to contain a fraction of points equal to $1 - \chi^2(k^2, n)$, where n is the dimension of the random variable.

In Figure 1.12, we see a two-dimensional ellipsoid generated according to $\mathcal{E} = \{Au \mid \|u\| \leq 1\}$, where

$$A = \begin{bmatrix} 1 & 2 \\ -1 & 3 \end{bmatrix}.$$

The one-, two-, and three-sigma ellipsoids are shown along with the minimum-volume ellipsoid containing these points.

We may generate an ellipsoid that covers a collection of points by using the mean as the center and an inflated covariance. While this method is very efficient numerically, it is possible to generate "smaller" ellipsoids using the methods of the next section.

1.5.2 Minimum-volume ellipsoid (MVE)

Let $\mathcal{S} = \{s_1, \ldots, s_m\} \in \mathbf{R}^{2n}$ be a set of possible values of the array manifold $a(\cdot)$. Assume $\mathcal{S}$ is bounded. In the case of a full rank ellipsoid, the problem of finding the minimum-volume ellipsoid containing the convex hull of $\mathcal{S}$ can be expressed as the following semidefinite program:

$$\begin{array}{ll} \text{minimize} & \log\det\ F^{-1} \\ \text{subject to} & F = F^T \succ 0 \\ & \|Fs_i - g\| \leq 1, \quad i = 1, \ldots, m. \end{array} \tag{1.62}$$

See Vandenberghe and Boyd [38] and Wu and Boyd [42]. The minimum-volume ellipsoid $\mathcal{E}$ containing $\mathcal{S}$ is called the *Löwner-John ellipsoid.* Equation (1.62) is a convex problem in variables F and g. For A full rank,

$$\{x \mid \|Fx - g\| \leq 1\} \;\equiv\; \{Au + c \mid \|u\| \leq 1\} \tag{1.63}$$

with $A = F^{-1}$ and $c = F^{-1}g$. The choice of A is not unique; in fact, any matrix of the form $F^{-1}U$ will satisfy (1.63), where U is any orthogonal matrix.

Commonly, $\mathcal{S}$ is well approximated by an affine set of dimension $l < 2n$ and (1.62) will be poorly conditioned numerically. We proceed by first applying a rank-preserving affine transformation $f : \mathbf{R}^{2n} \rightarrow \mathbf{R}^l$ to the elements of $\mathcal{S}$, with $f(s) = U_1^T(s - s_1)$. The matrix U_1 consists of the l left singular vectors, corresponding to the nonzero singular values, of the $2n \times (m-1)$ matrix

$$[(s_2 - s_1)\,(s_3 - s_1) \cdots (s_m - s_1)].$$

We may then solve (1.62) for the minimum-volume, non-degenerate ellipsoid in $\mathbf{R}^l$ that covers the image of $\mathcal{S}$ under f. The resulting ellipsoid can be described in $\mathbf{R}^{2n}$ as $\mathcal{E} = \{Au + c \mid \|u\| \leq 1\}$, with

$$A = U_1 F^{-1}$$

and

$$c = U_1 F^{-1} g + s_1.$$

For an l-dimensional ellipsoid description, a minimum of $l + 2$ points are required; *i.e.*, $m \geq l + 2$.

Compared to an ellipsoid based on the first- and second-order statistics, a minimum-volume ellipsoid is robust in the sense that it is guaranteed to cover all the data points used in the description; the MVE is *not* robust to data outliers. The computation of the covering ellipsoid is relatively complex; see Vandenberghe et al. [39]. In applications where a real-time response is required, the covering ellipsoid calculations may be profitably performed in advance and stored in a table.

In the next section, our philosophy is different. Instead of computing ellipsoid descriptions to describe collections of points, we consider operations on ellipsoids. While it is possible to develop tighter ellipsoidal approximations using the methods just described, the computational burden of these methods often precludes their use.

1.6 UNCERTAINTY ELLIPSOID CALCULUS

1.6.1 Union of ellipsoids

Suppose the actual AOA could assume one of p values and associated with each of these AOAs was an uncertainty ellipsoid. The possible values of the array manifold would be covered by the union of these ellipsoids. The resulting prob-

lem is then to find the "smallest" ellipsoid $\mathcal{E}_0$ that covers the union of ellipsoids, $\mathcal{E}_1(c_1, Q_1), \ldots, \mathcal{E}_p(c_p, Q_p)$. As in (1.16), we will describe these ellipsoids in terms of the associated quadratic functions

$$T_i(x) = x^T F_i x + 2x^T g_i + h_i,$$

where

$$F_i(x) = Q^{-1}, \quad g_i = -Q^{-1}c, \quad \text{and} \quad h_i = c^T Q^{-1} c - 1.$$

By the $\mathcal{S}-$procedure [7, pp23-24], $\mathcal{E}_i \subseteq \mathcal{E}_0$ for $i = 1, \ldots, p$ if and only if there exists non-negative scalars $\tau_1, \ldots, \tau_p$ such that

$$T_0(x) - \tau_i T_i(x) \leq 0, \quad i = 1, \ldots, p,$$

or equivalently, such that

$$\begin{bmatrix} F_0 & g_0 & 0 \\ g_0^T & -1 & g_0^T \\ 0 & g_0 & -F_0 \end{bmatrix} - \tau_i \begin{bmatrix} F_i & g_i & 0 \\ g_i^T & h_i & 0 \\ 0 & 0 & 0 \end{bmatrix} \leq 0,$$

for $i = 1, \ldots, p$. We can find the MVE containing the union of ellipsoids $\mathcal{E}_1, \ldots, \mathcal{E}_p$ by solving the matrix completion problem:

$$\begin{array}{ll} \text{minimize} & \log \det F_0^{-1} \\ \text{subject to} & F_0 > 0, \\ & \tau_1 \geq 0, \ldots, \tau_p \geq 0, \\ \multicolumn{2}{c}{\begin{bmatrix} F_0 & g_0 & 0 \\ g_0^T & -1 & g_0^T \\ 0 & g_0 & -F_0 \end{bmatrix} - \tau_i \begin{bmatrix} F_i & g_i & 0 \\ g_i^T & h_i & 0 \\ 0 & 0 & 0 \end{bmatrix} \leq 0,} \end{array}$$

for $i = 1, \ldots, p$, with variables F_0, g_0, and $\tau_1, \ldots, \tau_p$ [7, pp43-44]. The MVE covering the union of ellipsoids is then given by $\mathcal{E}(-F_0^{-1}g_0, F_0^{-2})$. An example of the minimum-volume ellipsoid covering the union of two ellipsoids in $\mathbf{R}^2$ is shown in Figure 1.13.

1.6.2 The sum of two ellipsoids

Recall that we can parameterize an ellipsoid in $\mathbf{R}^n$ in terms of its center $c \in \mathbf{R}^n$ and a symmetric non-negative definite configuration matrix $Q \in \mathbf{R}^{n \times n}$ as

$$\mathcal{E}(c, Q) = \{Q^{1/2}u + c \mid \|u\| \leq 1\},$$

where $Q^{1/2}$ is any matrix square root satisfying $Q^{1/2}(Q^{1/2})^T = Q$. Let $x \in \mathcal{E}_1 = \mathcal{E}(c_1, Q_1)$ and $y \in \mathcal{E}_2 = \mathcal{E}(c_2, Q_2)$. The range of values of the geometrical (or

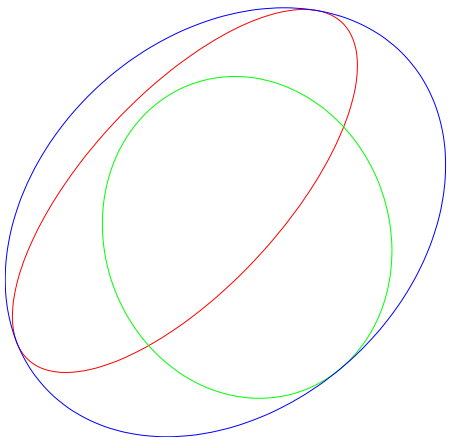

Fig. 1.13 A minimum-volume ellipsoid covering the union of two ellipsoids.

Minkowski) sum $z = x + y$ is contained in the ellipsoid

$$\mathcal{E} = \mathcal{E}(c_1 + c_2, Q(p)) \tag{1.64}$$

for all $p > 0$, where

$$Q(p) = (1 + p^{-1})Q_1 + (1 + p)Q_2; \tag{1.65}$$

see Kurzhanski and Vályi [26]. The value of p is commonly chosen to minimize either the determinant of $Q(p)$ or the trace of $Q(p)$. An example of the geometrical sum of two ellipses for various values of p is shown in Figure 1.14.

1.6.2.1 Minimum volume If $Q_1 \succ 0$ and $Q_2 \succ 0$, there exists a unique ellipsoid of minimal volume that contains the sum $\mathcal{E}_1 + \mathcal{E}_2$. It is described by $\mathcal{E}(c_1 + c_2, Q(p^*))$, where $p^* \in (0, \infty)$ is the unique solution of the equation

$$f(p) = \sum_{i=1}^{n} \frac{1}{\lambda_i + p} - \frac{n}{p(p+1)} = 0. \tag{1.66}$$

Here, $0 < \lambda_i < \infty$ are the roots of the equation $\det(Q_1 - \lambda Q_2) = 0$, *i.e.*, the generalized eigenvalues of Q_1 and Q_2 [26, pp.133-135]. The generalized eigenvalues can be determined by computing the eigenvalues of the matrix $Q_2^{-1/2} Q_1 (Q_2^{-1/2})^T$. Using the methods of §1.3, the solution of (1.66) may be found efficiently using Newton's method. In the event that neither Q_1 nor Q_2 is positive definite, but their sum is, a line search in p may be used to find the minimum-volume ellipsoid.

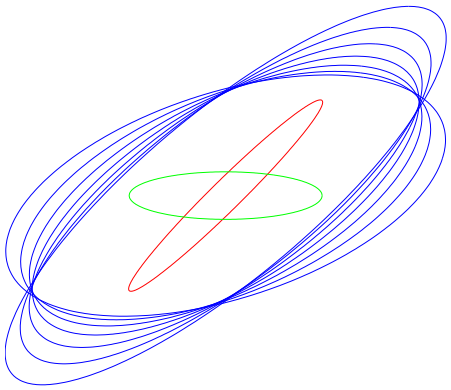

Fig. 1.14 Outer approximations of the sum of two ellipses (center) for different configuration matrices $Q(p) = (1 + 1/p)Q_1 + (1 + p)Q_2$.

1.6.2.2 Minimum trace There exists an ellipsoid of minimum trace, *i.e.*, sum of squares of the semiaxes, that contains the sum $\mathcal{E}_1(c_1, Q_q)+\mathcal{E}_2(c_2, Q_2)$; it is described by $\mathcal{E}(c_1 + c_2, Q(p^\star))$, where $Q(p)$ is as in (1.65),

$$p^\star = \sqrt{\frac{\mathbf{Tr}\, Q_1}{\mathbf{Tr}\, Q_2}}, \tag{1.67}$$

and **Tr** denotes trace. This fact, noted by Kurzhanski and Vályia [26, §2.5], may be verified by direct calculation.

Minimizing the trace of Q in equation (1.65) affords two computational advantages over minimizing the determinant. First, computing the optimal value of p can be done with $\mathcal{O}(n)$ operations; minimizing the determinant requires $\mathcal{O}(n^3)$. Second, the minimum-trace calculation is well-posed with degenerate ellipsoids.

1.6.3 An outer approximation to the Hadamard product of two ellipsoids

In practice, the output of the antenna array is often subject to uncertainties that are multiplicative in nature. These may be due to gains and phases of the electronics paths that are not precisely known. The gains may be known to have some formal uncertainty; in other applications, these quantities are estimated in terms of a mean vector and covariance matrix. In both cases, this uncertainty is well-described by an ellipsoid; this is depicted schematically in Figure 1.15.

Assume that the range of possible values of the array manifold is described by an ellipsoid $\mathcal{E}_1 = \{Au+b \mid \|u\| \leq 1\}$. Similarly assume the multiplicative uncertainties lie within a second ellipsoid $\mathcal{E}_2 = \{Cv + d \mid \|v\| \leq 1\}$. The set of possible values of the array manifold in the presence of multiplicative uncertainties is described by

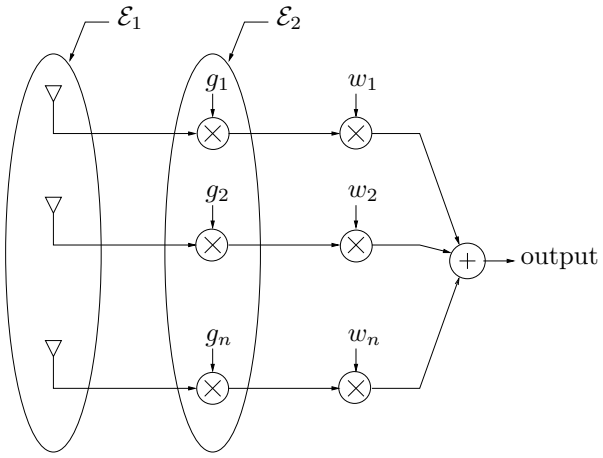

Fig. 1.15 The possible values of array manifold are contained in ellipsoid $\mathcal{E}_1$; the values of gains are described by ellipsoid $\mathcal{E}_2$. The design variable w needs to consider the multiplicative effect of these uncertainties.

the numerical range of the Hadamard, *i.e.*, element-wise product of $\mathcal{E}_1$ and $\mathcal{E}_2$. We will develop outer approximations to the Hadamard product of two ellipsoids. In §1.6.5, we consider the case where both ellipsoids describe real numbers; the case of complex values is considered in §1.6.6. Prior to this, we will review some basic facts about Hadamard products.

1.6.4 Preliminaries

Lemma 3 *For any* $x, y \in \mathbf{R}^n$,

$$(x \circ y)(x \circ y)^T = (xx^T) \circ (yy^T).$$

Proof: Direct calculation shows that the i, j entry of the product is $x_i y_i x_j y_j$, which can be regrouped as $x_i x_j y_i y_j$. □

Lemma 4 *Let* $x \in \mathcal{E}_x = \{Au \mid \|u\| \leq 1\}$ *and* $y \in \mathcal{E}_y = \{Cv \mid \|v\| \leq 1\}$. *The field of values of the Hadamard product* $x \circ y$ *is contained in the ellipsoid*

$$\mathcal{E}_{xy} = \{(AA^T \circ CC^T)^{1/2} w \mid \|w\| \leq 1\}.$$

Proof: By Lemma 3 we have

$$(x \circ y)(x \circ y)^T = (xx^T) \circ (yy^T).$$

In particular,

$$(Au \circ Cv)(Au \circ Cv)^T = (Auu^T A^T) \circ (Cvv^T C^T).$$

Expanding $AA^T \circ CC^T$ as:

$$\begin{aligned} AA^T \circ CC^T &= A(uu^T)A^T \circ C(vv^T)C^T \\ &+ A(uu^T)A^T \circ C(I_n - vv^T))C^T \\ &+ A(I_n - uu^T)A^T \circ C(vv^T)C^T \\ &+ A(I_n - uu^T)A^T \circ C(I_n - vv^T)C^T, \end{aligned} \tag{1.68}$$

we see the Hadamard product of two positive semidefinite matrices is also positive semidefinite [21, pp.298-301]. Therefore,

$$(AA^T \circ CC^T) \succeq (Au \circ Cv)(Au \circ Cv)^T \; \forall \, \|u\| \leq 1, \|v\| \leq 1.$$

□

Lemma 5 *Let $\mathcal{E}_1 = \{Au \mid \|u\| \leq 1\}$ and let d be any vector in $\mathbf{R}^n$. The Hadamard product of $\mathcal{E}_1 \circ d$ is contained in the ellipsoid*

$$\mathcal{E} = \{(AA^T \circ dd^T)^{1/2} w \mid \|w\| \leq 1\}.$$

Proof: This is simply a special case of Lemma 3. □

1.6.5 Outer approximation

Let $\mathcal{E}_1 = \{Au + b \mid \|u\| \leq 1\}$ and $\mathcal{E}_2 = \{Cv + d \mid \|v\| \leq 1\}$ be ellipsoids in $\mathbf{R}^n$. Let x and y be n dimensional vectors taken from ellipsoids $\mathcal{E}_1$ and $\mathcal{E}_2$, respectively. Expanding the Hadamard product $x \circ y$, we have:

$$x \circ y = b \circ d + Au \circ Cv \; + Au \circ d + b \circ Cv. \tag{1.69}$$

By Lemmas 4 and 5, the field of values of the Hadamard product

$$x \circ y \in \{(Au + b) \circ (Cv + d) \mid \|u\| \leq 1, \|v\| \leq 1\}$$

is contained in the geometrical sum of three ellipsoids

$$\begin{aligned} \mathcal{S} &= \mathcal{E}(b \circ d, AA^T \circ CC^T) + \\ &\quad \mathcal{E}(0, AA^T \circ dd^T) + \mathcal{E}(0, bb^T \circ CC^T). \end{aligned} \tag{1.70}$$

Ignoring the correlations between terms in the above expansion, we find that $\mathcal{S} \subseteq \mathcal{E}(b \circ d, Q)$, where

$$\begin{aligned} Q &= (1 + 1/p_1)\,(1 + 1/p_2)\,AA^T \circ CC^T + \\ &\quad (1 + p_1)\,(1 + 1/p_2)\,AA^T \circ dd^T + \\ &\quad (1 + p_1)\,(1 + p_2)\,CC^T \circ bb^T \end{aligned} \tag{1.71}$$

for all $p_1 > 0$ and $p_2 > 0$. The values of p_1 and p_2 may be chosen to minimize the trace or the determinant of Q. The trace metric requires far less computational

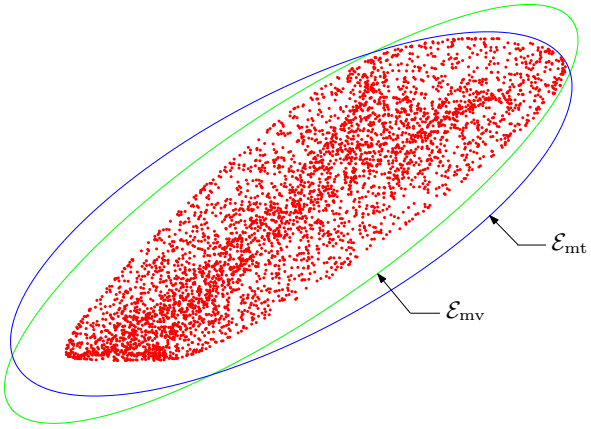

Fig. 1.16 Samples of the Hadamard product of two ellipsoids. The outer approximations based on the minimum-volume and minimum-trace metrics are labeled $\mathcal{E}_{\mathrm{mv}}$ and $\mathcal{E}_{\mathrm{mt}}$.

effort and is numerically more reliable; if either b or d has a very small entry, the corresponding term in expansion (1.71) will be poorly conditioned.

As a numerical example, we consider the Hadamard product of two ellipsoids in $\mathbf{R}^2$. The ellipsoid $\mathcal{E}_1$ is described by

$$A = \begin{bmatrix} -0.6452 & -1.5221 \\ 0.2628 & 2.2284 \end{bmatrix}, \; b = \begin{bmatrix} -5.0115 \\ 1.8832 \end{bmatrix};$$

the parameters of $\mathcal{E}_2$ are

$$C = \begin{bmatrix} -1.0710 & 0.7919 \\ 0.8744 & 0.7776 \end{bmatrix}, \; d = \begin{bmatrix} -9.5254 \\ 9.7264 \end{bmatrix}.$$

Samples of the Hadamard product of $\mathcal{E}_1 \circ \mathcal{E}_2$ are shown in Figure 1.16 along with the outer approximations based on the minimum-volume and minimum-trace metrics; more Hadamard products of ellipsoids and outer approximations are shown in Figures 1.17 and 1.18.

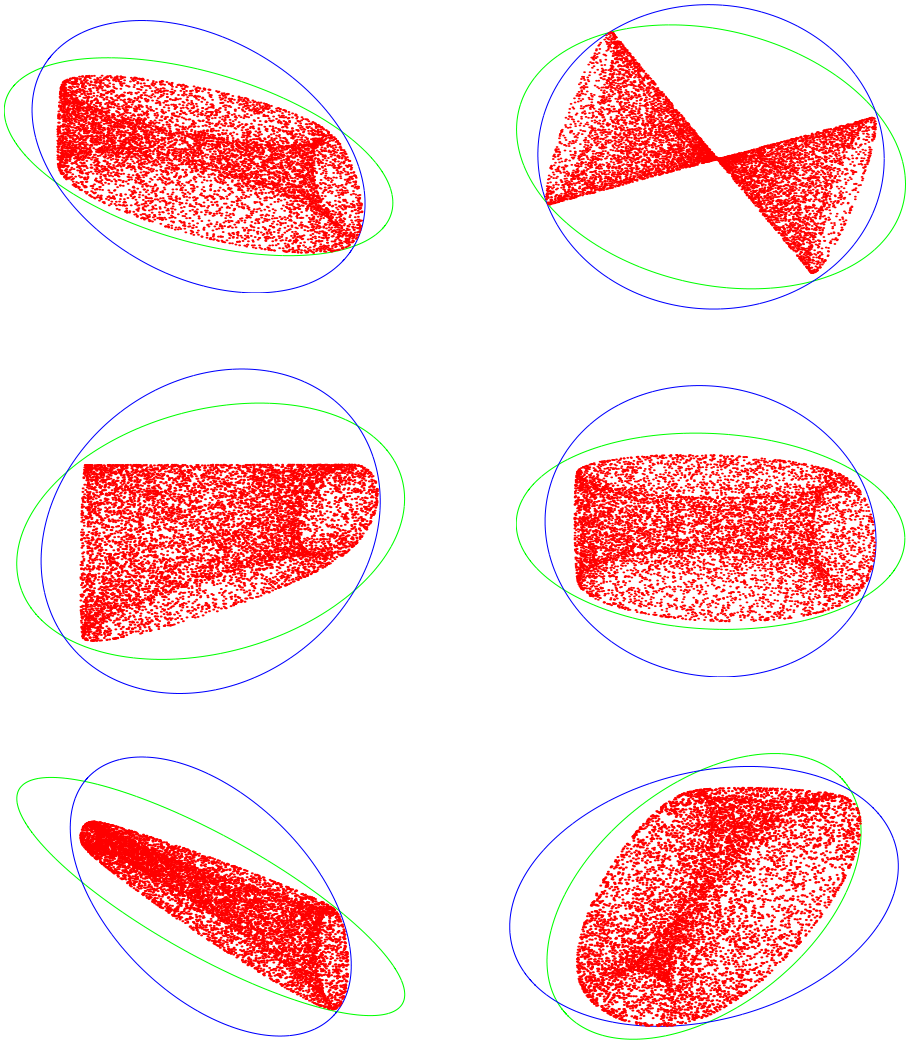

Fig. 1.17 The Hadamard product of ellipsoids.

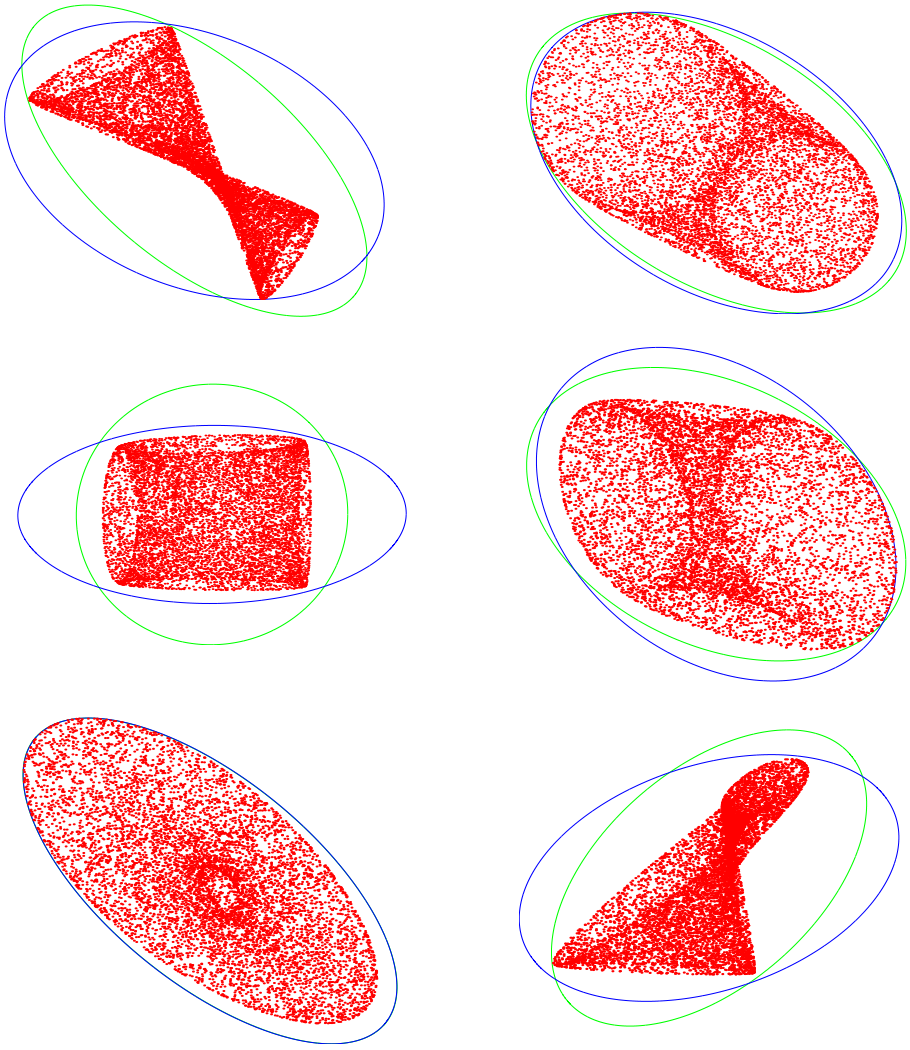

Fig. 1.18 More Hadamard products of ellipsoids.

1.6.6 The complex case

We now extend the results of §1.6.5 to the case of complex values. For numerical efficiency, we compute the approximating ellipsoid using the minimum-trace metric. As before, we represent complex numbers by the direct sum of their real and imaginary components. Let $x \in \mathbf{R}^{2n}$ and $y \in \mathbf{R}^{2n}$ be the direct-sum representations of $\alpha \in \mathbf{C}^n$ and $\beta \in \mathbf{C}^n$, respectively; *i.e.*,

$$x = \begin{bmatrix} \mathbf{Re}\,\alpha \\ \mathbf{Im}\,\alpha \end{bmatrix}, \qquad y = \begin{bmatrix} \mathbf{Re}\,\beta \\ \mathbf{Im}\,\beta \end{bmatrix}.$$

We can represent the real and imaginary components of $\gamma = \alpha \circ \beta$ as

$$\begin{aligned} z &= \begin{bmatrix} \mathbf{Re}\,\gamma \\ \mathbf{Im}\,\gamma \end{bmatrix} \\ &= \begin{bmatrix} \mathbf{Re}\,\alpha \circ \mathbf{Re}\,\beta - \mathbf{Im}\,\alpha \circ \mathbf{Im}\,\beta \\ \mathbf{Im}\,\alpha \circ \mathbf{Re}\,\beta + \mathbf{Re}\,\alpha \circ \mathbf{Im}\,\beta \end{bmatrix} \\ &= F_1 x \circ F_2 y + F_3 x \circ F_4 y, \end{aligned} \tag{1.72}$$

where

$$F_1 = \begin{bmatrix} I_n & 0 \\ 0 & I_n \end{bmatrix}, \quad F_2 = \begin{bmatrix} I_n & 0 \\ I_n & 0 \end{bmatrix},$$

and

$$F_3 = \begin{bmatrix} 0 & -I_n \\ I_n & 0 \end{bmatrix}, \quad F_4 = \begin{bmatrix} 0 & I_n \\ 0 & I_n \end{bmatrix}.$$

The multiplications associated with matrices $F_1, \ldots, F_4$ are achieved with a reordering of the calculations. Applying (1.72) to $x \in \mathcal{E}_1 = \{Au + b \mid \|u\| \leq 1\}$ and $y \in \mathcal{E}_2 = \{Cv + d \mid \|v\| \leq 1\}$ yields:

$$\begin{aligned} z \;=\; & F_1 b \circ F_2 d + \\ & F_3 b \circ F_4 d + \\ & F_1 Au \circ F_2 Cv + \\ & F_1 Au \circ F_2 d + \\ & F_1 b \circ F_2 Cv + \\ & F_3 Au \circ F_4 Cv + \\ & F_3 Au \circ F_4 d + \\ & F_3 b \circ F_4 Cv. \end{aligned} \tag{1.73}$$

The direct-sum representation of the field of values of the complex Hadamard product $\alpha \circ \beta$ is contained in the geometrical sum of ellipsoids

$$\begin{aligned} \mathcal{S} \quad = \quad & \mathcal{E}(F_1 b \circ F_2 d, F_1 A A^T F_1^T \circ F_2 C C^T F_2^T) + \\ & \mathcal{E}(F_3 b \circ F_4 d, F_1 A A^T F_1^T \circ F_2 d d^T F_2^T) + \\ & \mathcal{E}(0, F_1 b b^T F_1^T \circ F_2 C C^T F_2^T) + \\ & \mathcal{E}(0, F_3 A A^T F_3^T \circ F_4 C C^T F_4^T) + \\ & \mathcal{E}(0, F_3 A A^T F_3^T \circ F_4 d d^T F_4^T) + \\ & \mathcal{E}(0, F_3 b b^T F_3^T \circ F_4 C C^T F_4^T). \end{aligned} \tag{1.74}$$

We compute $\mathcal{E}(c, Q) \supseteq \mathcal{S}$, where the center of the covering ellipsoid is given by the sum of the first two terms of (1.73). The configuration matrix Q is calculated by repeatedly applying (1.64) and (1.65) to the remaining terms of (1.73), where p is chosen according to (1.67).

1.6.7 An improved approximation

We now make use of two facts that generally lead to tighter approximations. First, the ellipsoidal outer approximation ignores any correlation between the terms in expansion (1.73); hence, it is productive to reduce the *number* of these terms.

Consider a Givens rotation matrix of the form:

$$T = \begin{bmatrix} \cos\theta_1 & & & \sin\theta_1 & & \\ & \ddots & & & \ddots & \\ & & \cos\theta_n & & & \sin\theta_n \\ -\sin\theta_1 & & & \cos\theta_1 & & \\ & \ddots & & & \ddots & \\ & & -\sin\theta_n & & & \cos\theta_n \end{bmatrix}. \tag{1.75}$$

The effect of pre-multiplying a direct sum-representation of a complex vector by T is to shift the phase of each component by the corresponding angle θ_i. It follows that for all T_x and T_y of the form (1.75) we have

$$\begin{aligned} & T_x^{-1} T_y^{-1} (F_1 T_x x \circ F_2 T_y y + F_3 T_x x \circ F_4 T_y y) = \\ & F_1 x \circ F_2 y + F_3 x \circ F_4 y, \end{aligned} \tag{1.76}$$

which does not hold for unitary matrices in general.

We now compute rotation matrices T_b and T_d such that the entries associated with the imaginary components of products $T_b b$ and $T_d d$ are zero. In computing T_b, we choose the values of θ in (1.75) according to $\theta_i = \angle(b(i) + \sqrt{-1} \times b(n+i))$. T_y is similarly computed using the values of d; *i.e.*, $\theta_i = \angle(d(i) + \sqrt{-1} \times d(n+i))$. We

change coordinates according to

$$\begin{array}{rcl} A & \leftarrow & T_b A \\ b & \leftarrow & T_b b \\ C & \leftarrow & T_d C \\ d & \leftarrow & T_d d. \end{array}$$

The rotated components associated with the ellipsoid centers have the form

$$T_b b = \begin{bmatrix} \tilde{b}_1 \\ \vdots \\ \tilde{b}_n \\ 0 \\ \vdots \\ 0 \end{bmatrix}, \quad T_d d = \begin{bmatrix} \tilde{d}_1 \\ \vdots \\ \tilde{d}_n \\ 0 \\ \vdots \\ 0 \end{bmatrix}, \tag{1.77}$$

zeroing the term $F_3 T_b A A^T T_b^T F_3^T \circ (F_4 T_d d d^T T_d^T F_4^T)$ in (1.73). The desired outer approximation is computed as the geometrical sum of outer approximations to the remaining five terms. That is,

$$\begin{array}{rl} \mathcal{E}(c,Q) \supseteq & \mathcal{E}(F_1 b \circ F_2 d, F_1 A A^T F_1^T \circ F_2 C C^T F_2^T) + \\ & \mathcal{E}(F_3 b \circ F_4 d, F_1 A A^T F_1^T \circ F_2 d d^T F_2^T) + \\ & \mathcal{E}(0, F_1 b b^T F_1^T \circ F_2 C C^T F_2^T) + \\ & \mathcal{E}(0, F_3 A A^T F_3^T \circ F_4 C C^T F_4^T) + \\ & \mathcal{E}(0, F_3 b b^T F_3^T \circ F_4 C C^T F_4^T). \end{array} \tag{1.78}$$

Second, while the Hadamard product is commutative, the outer approximation based on covering the individual terms in the expansion (1.73) *is* sensitive to ordering; simply interchanging the dyads $\{A, b\}$ and $\{C, d\}$ results in different qualities of approximations. The ellipsoidal approximation associated with this interchanged ordering is given by:

$$\begin{array}{rl} \mathcal{E}(c,Q) \supseteq & \mathcal{E}(F_1 d \circ F_2 b, F_1 C C^T F_1^T \circ F_2 A A^T F_2^T) + \\ & \mathcal{E}(F_3 d \circ F_4 b, F_1 C C^T F_1^T \circ F_2 b b^T F_2^T) + \\ & \mathcal{E}(0, F_1 d d^T F_1^T \circ F_2 A A^T F_2^T) + \\ & \mathcal{E}(0, F_3 C C^T F_3^T \circ F_4 A A^T F_4^T) + \\ & \mathcal{E}(0, F_3 d d^T F_3^T \circ F_4 A A^T F_4^T). \end{array} \tag{1.79}$$

Since our goal is to find the smallest ellipsoid covering the numerical range of z, we compute the trace associated with both orderings and choose the smaller of the two. This determination can be made without computing the minimum-trace ellipsoids explicitly. Let $\mathcal{E}_0$ be the minimum-trace ellipsoid covering $\mathcal{E}_1 + \cdots + \mathcal{E}_p$. The trace

of $\mathcal{E}_0$ is given by:

$$\mathbf{Tr}\,\mathcal{E}_0 = \left(\sqrt{\mathbf{Tr}\,\mathcal{E}_1} + \sqrt{\mathbf{Tr}\,\mathcal{E}_2} + \cdots + \sqrt{\mathbf{Tr}\,\mathcal{E}_p}\right)^2,$$

which may be verified by direct calculation. Hence, determining which of (1.78) and (1.79) yields the smaller trace can be performed in $\mathcal{O}(n)$ calculations. After making this determination, we perform the remainder of the calculations to compute the desired configuration matrix Q. We then transform Q back to the original coordinates according to:

$$Q \leftarrow (T_b^{-1}T_d^{-1})Q(T_b^{-1}T_d^{-1})^T.$$

1.7 EXAMPLE OF BEAMFORMING IN PRESENCE OF MULTIPLICATIVE UNCERTAINTIES

Consider a six-element uniform linear array, centered at the origin, in which the spacing between the elements is half of a wavelength whose response is given by:

$$a(\theta) = \left[\begin{array}{cccccc} e^{-5\phi/2} & e^{-3\phi/2} & \ldots & e^{3\phi/2} & e^{5\phi/2} \end{array}\right]^T,$$

where $\phi = \pi\cos(\theta)$ and θ is the angle of arrival.

As in the previous example, three signals impinge upon the array: a desired signal $s_{\rm d}(t)$ and two uncorrelated interfering signals $s_{\rm int1}(t)$ and $s_{\rm int2}$. The signal-to-noise ratio (SNR) of the desired signal at each element is 20 dB. The angles of arrival of the interfering signals, $\theta_{\rm int1}$ and $\theta_{\rm int2}$, are 30° and 75°; the SNRs of these interfering signals, 40dB and 20dB, respectively. The received signals are modeled as in (1.57). The signals pass through an amplification stage as depicted in Fig.1.6.3. The gain vector $g \in \mathbf{C}^6$ is chosen from the ellipsoid which we represent, in terms of the direct sum of the real and imaginary components in $\mathbf{R}^{12}$ according to $\mathcal{E}_g = \mathcal{E}(Q_g, c_g)$, where

$$Q_g = \left[\begin{array}{cc} Q_d & \\ & Q_d \end{array}\right], \quad c_g = \left[\begin{array}{cccccc} 1 & \ldots & 1 & 0 & \ldots & 0 \end{array}\right]^T,$$

and Q_d is a diagonal matrix, the ith diagonal element of which equals 10^{-i}. Given the symmetry in the uncertainty region of the present example, the set of possible values of $g \in \mathbf{C}^6$ also satisfy $(g^* - \mathbf{1})Q_d^{-1}(g^* - \mathbf{1})$, where $\mathbf{1}$ is a vector of ones.

As in §1.4, the actual array response is contained in an ellipsoid $\mathcal{E}_a(c, P)$, whose center and configuration matrix are computed from 64 equally-spaced samples of the array response at angles between 40° and 50° according to (1.59), (1.60).

The aggregate uncertainty in the Hadamard product of the array manifold and the gain vector is then given by the (complex) Hadamard product of the above uncertainty ellipsoids. We compute an ellipsoidal outer approximation to this aggregate uncertainty ellipsoid, using the methods of §1.6.6 and §s-ellipsoid-multiplicative-improved, *viz.*: $\mathcal{E}_a(c, P) \subset \mathcal{E}_g \circ \mathcal{E}_a$.

We will use an analytically computed, expected covariance which again uses the actual array response and which assumes that the signals $s_{\mathrm{d}}(t), s_{\mathrm{int1}}(t), s_{\mathrm{int2}}(t)$, and $v(t)$ are all uncorrelated and that the additive noise is applied at the output of the amplification stage. The covariance is modeled as:

$$\begin{aligned} \mathbf{E}\, R = \mathbf{E}\, yy^* = \quad & \sigma_{\mathrm{d}}^2 (g \circ a_{\mathrm{d}})(g \circ a_{\mathrm{d}})^* + \\ & \sigma_{\mathrm{int1}}^2 \left(g \circ a(\theta_{\mathrm{int1}})\right) \left(g \circ a(\theta_{\mathrm{int1}})\right)^* + \\ & \sigma_{\mathrm{int2}}^2 \left(g \circ a(\theta_{\mathrm{int2}})\right) \left(g \circ a(\theta_{\mathrm{int2}})\right)^* + \\ & \sigma_{\mathrm{n}}^2 I. \end{aligned} \tag{1.80}$$

The worst-case SINR is the minimum objective value of the following optimization problem:

$$\begin{array}{ll} \text{minimize} & \dfrac{\sigma_{\mathrm{d}}^2 \|w^*(g \circ a)\|^2}{\mathbf{E}\, w^* R_v w} \\ \text{subject to} & a \in \mathcal{E}(c, P); \end{array}$$

where the expected covariance of the interfering signals and noises is given by

$$\mathbf{E}\, R_v = \sigma_{\mathrm{int1}}^2 (g \circ a(\theta_{\mathrm{int1}}))(g \circ a(\theta_{\mathrm{int1}})^* + \sigma_{\mathrm{int1}}^2 (g \circ a(\theta_{\mathrm{int2}}))(g \circ a(\theta_{\mathrm{int2}}))^* + \sigma_{\mathrm{n}}^2 I.$$

The weight vector w and covariance matrix of the noise and interfering signals R_v used in its computation reflect the chosen values of the gain vector and array manifold. We will consider four cases:

1 The assumed and actual gains are nominal (unity).

2 The gain, assumed and actual, can assume any value in $\mathcal{E}_g$.

3 The gain is assumed to vary within $\mathcal{E}_a$; the actual gain is nominal.

4 The gain is assumed nominal, but can assume any value in $\mathcal{E}_g$.

The beamformers and worst-case SINRs for these cases were computed to be:

$$\text{case } 1: \qquad w_1 = \begin{bmatrix} -0.1760 + 0.1735i \\ -1.1196 + 0.5592i \\ -0.4218 + 0.4803i \\ -0.4245 - 0.4884i \\ -1.1173 - 0.5598i \\ -0.1720 - 0.1767i \end{bmatrix}, \quad \text{SINR} = 14.26\text{dB}$$

$$\text{case } 2: \qquad w_2 = \begin{bmatrix} 0.0350 + 0.0671i \\ -0.6409 - 0.0109i \\ 0.2388 - 0.3422i \\ 1.1464 - 1.1488i \\ 0.2749 - 2.1731i \\ 0.0201 - 1.2138i \end{bmatrix}, \quad \text{SINR} = 11.22\text{dB},$$

$$\text{case } 3: \qquad w_3 = \begin{bmatrix} 0.0418 + 0.0740i \\ -0.6248 + 0.0241i \\ 0.2579 - 0.3097i \\ 1.1192 - 1.1111i \\ 0.2445 - 2.0927i \\ 0.0317 - 1.1681i \end{bmatrix}, \quad \text{SINR} = 11.30\text{dB},$$

$$\text{case } 4: \qquad w_4 = \begin{bmatrix} 0.9141 + 2.6076i \\ 2.4116 + 1.6939i \\ -0.1105 - 0.1361i \\ -0.6070 + 1.2601i \\ -0.4283 - 0.8408i \\ -1.1158 - 1.0300i \end{bmatrix}, \quad \text{SINR} = -2.81\text{dB}.$$

In the first case, the gains nominal and actual are unity; the worst-case SINR is seen to be 14.26 dB. In the second case, the gain is allowed to vary; not surprisingly, the worst- case SINR decreases to 11.22dB. In the third case, the beamformer is computed assuming possible variation in the gains when in fact, there is none. The worst-case SINR in this case is 11.30 dB, quite close to that of the second case. The interpretation is that robustness comes at the expense of nominal performance. In the last case, the uncertainty ellipsoid used in the beamformer computation underestimated the aggregate uncertainty; this optimism is seen to be punished.

The uncertainty in the gain for the first antenna element is large, for the last, small, and for the middle elements, somewhere in between. When this possible gain variation is factored into the aggregate uncertainty ellipsoid, the RMVB based on this aggregate ellipsoid discounts the information in the less reliable measurements by assigning

to them small (in absolute value) weights. This is seen in the first and (to a lesser extent) the second entries of beamformer vectors w_2 and w_3.

1.8 SUMMARY

The main ideas of our approach are as follows:

- The possible values of the manifold are approximated or covered by an ellipsoid that describes the uncertainty.
- The robust minimum variance beamformer is chosen to minimize the weighted power out of the array subject to the constraint that the gain is greater than unity for all array manifold values in the ellipsoid.
- The RMVB can be computed very efficiently using Lagrange multiplier techniques.
- Ellipsoidal calculus techniques may be used to efficiently propagate the uncertainty ellipsoid in the presence of multiplicative uncertainties.

GLOSSARY

Appendix: Notation and Glossary

$\mathbf{R}$	The set of real numbers.
$\mathbf{R}^m$	The set of real m-vectors.
$\mathbf{R}^{m\times n}$	The set of real $m \times n$ matrices.
$\mathbf{C}$	The set of complex numbers.
$\mathbf{C}^m$	The set of complex m-vectors.
$\mathbf{C}^{m\times n}$	The set of complex $m \times n$ matrices.
$\mathbf{Tr}\, X$	The trace of X.
$\mathbf{E}\, X$	The expected value of X.
$\det X$	The determinant of X.
$\|x\|$	The Euclidean (l_2) norm of x.
I	The identity matrix (of appropriate dimensions).
$x \circ y$	The Hadamard or element-wise product of x and y.
$X \succ 0$ ($X \succeq 0$)	X is positive (semi-)definite, *i.e.*, $X = X^T$ and $z^T X z > 0$ ($z^T X z \geq 0$) for all nonzero z.
$X \succ Y$ ($X \succeq Y$)	$X - Y$ is positive (semi-)definite.

A/D	Analog to Digital Converter
AOA	Angle of Arrival
dB	decibel
MVE	Minimum-Volume Ellipsoid
LNA	Low-Noise Amplifier
MVB	Minimum-Variance Beamformer
NEC	Numerical Electromagnetics Code
RF	Radio Frequency
RMVB	Robust Minimum Variance Beamformer
SINR	Signal-to-Interference-plus-Noise Ratio
SNR	Signal-to-Noise Ratio

Index

References

1. Y. I. Abromovich and M. B. Sverdlik. Synthesis of a filter which maximizes the signal-to-noise ratio under additional quadratic constraints. *Radio Eng. and Electron. Phys.*, 15(11):1977–1984, Nov. 1970.

2. A. Ben-Tal, L. El Ghaoui, and A. Nemirovski. Robustness. In *Handbook on Semidefinite Programming*, chapter 6, pages 138–162. Kluwer, Boston, 2000.

3. A. Ben-Tal and A. Nemirovski. Robust convex optimization. *Mathematics of Operations Research*, 23(4):769–805, 1998.

4. A. Ben-Tal and A. Nemirovski. Robust solutions of uncertain linear programs. *Operations Research Letters*, 25(1):1–13, 1999.

5. A. Ben-Tal and A. Nemirovski. *Lectures on Modern Convex Optimization: Analysis, Algorithms, and Engineering Applications*. MPS/SIAM Series on Optimization. SIAM, Philadelphia, 2001.

6. D. P. Bertsekas. *Constrained Optimization and Lagrange Multiplier Methods*. Athena Scientific, Belmont, MA, 1996.

7. S. P. Boyd, L. El Ghaoui, E. Feron, and V. Balakrishnan. *Linear Matrix Inequalities in System and Control Theory*, volume 15 of *Studies in Applied Mathematics*. SIAM, Philadelphia, Jun. 1994.

8. S. P. Boyd and L. Vandenberghe. *Convex Optimization*. Cambridge University Press, Cambridge, UK, 2004.

9. G. J. Burke. Numerical Electromagnetics Code - NEC-4 Method of Moments. Technical Report UCRL-MA-109338, Lawrence Livermore National Laboratory, Jan. 1992.

10. J. Capon. High-resolution frequency-wavenumber spectrum analysis. *Proc. IEEE*, 57(8):1408–1418, Aug. 1969.

11. G. Dahlquist and Å. Björck. *Numerical Methods*. Series in Automatic Computation. Prentice Hall, Englewood Cliffs, New Jersey, 1974.

12. J. W. Demmel. *Applied Numerical Linear Algebra*. SIAM, Philadelphia, 1997.

13. L. El Ghaoui and H. Lebret. Robust solutions to least-squares problems with uncertain data. *SIAM J. on Matrix Anal. Appl.*, 18(4):1035–1064, Oct. 1997.

14. W. Gander. Least squares with a quadratic constraint. *Numerische Mathematik*, 36(3):291–307, Feb. 1981.

15. A. B. Gershman. Robust adaptive beamforming in sensor arrays. *AEU-International Journal of Electronics and Communication*, 53(6):305–314, Dec. 1999.

16. A. B. Gershman, Z-Q Luo, S. Shahbazpanahi, and S. Vorobyov. Robust adaptive beamforming based on worst-case performance optimization. In *The Thirty-Seventh Asilomar Conference on Signals, Systems, and Computers*, pages 1353–1357, 2003.

17. G. H. Golub and C. Van Loan. *Matrix Computations*. Johns Hopkins Univ. Press, Baltimore, 2nd edition, 1989.

18. G. H. Golub and U. von Matt. Quadratically constrained least squares and quadratic problems. *Numerische Mathematik*, 59(1):561–580, Feb. 1991.

19. K. Harmanci, J. Tabrikian, and J. L. Krolik. Relationships between adaptive minimum variance beamforming and optimal source localization. *IEEE Transactions on Signal Processing*, 48(1):1–13, Jan. 2000.

20. S. Haykin. *Adaptive Filter Theory*. Prentice Hall information and system sciences series. Prentice Hall, Englewood Cliffs, 1996.

21. R. Horn and C. Johnson. *Topics in Matrix Analysis*. Cambridge University Press, Cambridge, 1991.

22. D. Johnson and D. Dudgeon. *Array Signal Processing: Concepts and Techniques*. Signal Processing Series. P T R Prentice Hall, Englewood Cliffs, 1993.

23. T. Kailath, A. H. Sayed, and B. Hassibi. *Linear Estimation*. Information and System Sciences Series. Prentice Hall, Upper Saddle River, NJ, 2000.

24. J. L. Krolik. Matched-field minimum variance beamforming. *J. Acoust. Soc. Am.*, 92(3):1406–1419, Sep. 1992.

25. J. L. Krolik. The performance of matched-field beamformers with Mediterranean vertical array data. *IEEE Transactions on Signal Processing*, 44(10):2605–2611, Jan. 1996.

26. A. Kurzhanski and I. Vályi. *Ellipsoidal Calculus for Estimation and Control*. Systems & Control: Foundations & Applications. Birkhauser, Boston, 1997.

27. H. Lebret and S. P. Boyd. Antenna array pattern synthesis via convex optimization. *IEEE Trans. Antennas Propag.*, 45(3):526–532, Mar. 1997.

28. J. Li, P. Stoica, and Z. Wang. Doubly constrained robust Capon beamformer. In *The Thirty-Seventh Asilomar Conference on Signals, Systems, and Computers*, volume 2, pages 1335–1339, 2003. (to appear in IEEE Transaction on Signal Processing).

29. J. Li, P. Stoica, and Z. Wang. On robust Capon beamforming and diagonal loading. *IEEE Transactions on Signal Processing*, 51(7):1702–1715, Jul. 2003.

30. M. S. Lobo, L. Vandenberghe, S. P. Boyd, and H. Lebret. Applications of second-order cone programming. *Linear Algebra and Applications*, 284(1-3):193–228, Nov. 1998.

31. R. Lorenz and S. Boyd. Robust minimum variance beamforming. In *The Thirty-Seventh Asilomar Conference on Signals, Systems, and Computers*, volume 2, pages 1345–1352, 2003.

32. R. G. Lorenz and S. P. Boyd. Robust beamforming in GPS arrays. In *Proc.Institute of Navigation, National Technical Meeting*, Jan. 2002.

33. R. G. Lorenz and S. P. Boyd. Robust minimum variance beamforming. *IEEE Transactions on Signal Processing*, 2002. to appear.

34. A. L. Soyster. Convex programming with set-inclusive constraints and applications to inexact linear programming. *Operations Research*, 21(5):1154–1157, Sep.-Oct. 1973.

35. P. Stoica, Z. Wang, and J. Li. Robust Capon beamforming. *IEEE Signal Processing Letters, volume = 10, number = 6, month = jun, pages = 172–175, year = 2003*.

36. C. A. Stutt and L. J. Spafford. A "best" mismatched filter response for radar clutter discrimination. *IEEE Transactions on Information Theory*, IT-14(2):280–287, Mar. 1968.

37. A. N. Tikhonov and Y. V. Arsenin. *Solution of Ill-Posed Problems*. V. H. Winston and Sons, 1977. Translated from Russian.

38. L. Vandenberghe and S. P. Boyd. Semidefinite programming. In *Siam Review*, 1995.

39. L. Vandenberghe, S. P. Boyd, and S.-P. Wu. Determinant maximization with linear matrix inequality constraints. *SIAM J. on Matrix Anal. Appl.*, 19(2):499–533, Apr. 1998.

40. S. A. Vorobyov, A. B. Gershman, and Z.-Q. Luo. Robust adaptive beamforming using worst-case performance optimization via second-order cone programming. In *Proc. IEEE International Conf. on Acoustics, Speech and Signal Processing*, volume III, 2002.